Figure S1. HPLC detection of aurachin RE in *rauA* gene complemented strain C02.

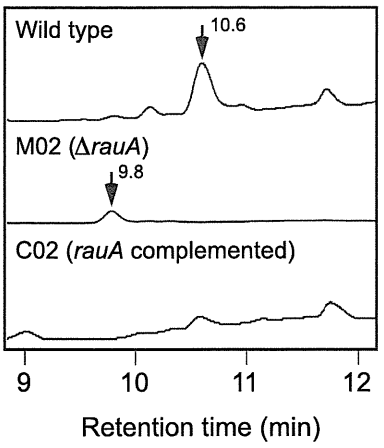

Figure S2. Structures of the biosynthetic intermediate of aurachin RE (**2**). COSY and HMBC correlations are shown in bold lines and arrows.

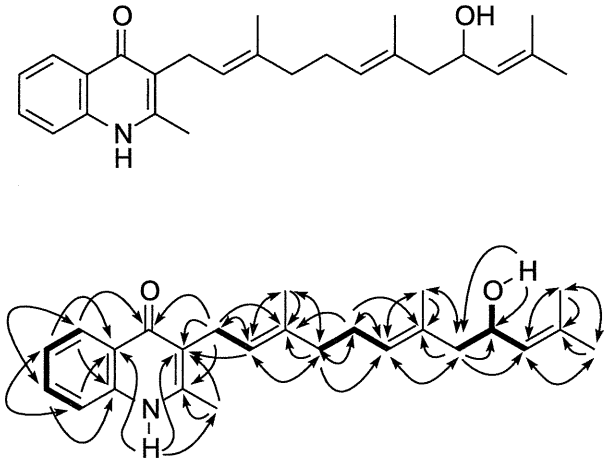

Figure S3. HPLC detection of aurachin RE and the intermediate. Aurachin RE (**1**: rt=10.6 min), and biosynthetic intermediate isolated from *rauA* mutant strain (**2**: rt=9.8 min).

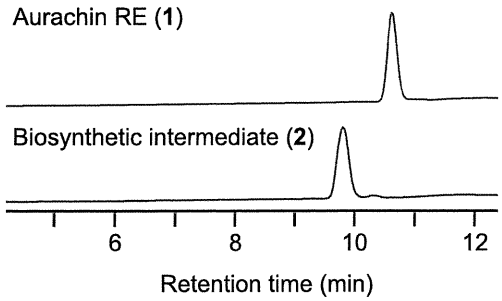

Figure S4. Organization of *rau* genes in gene disrupted mutant strain (M01-M11). Deleted nucleotide region in each *rau* gene mutant strain was indicated with bold line above each of the ORF.

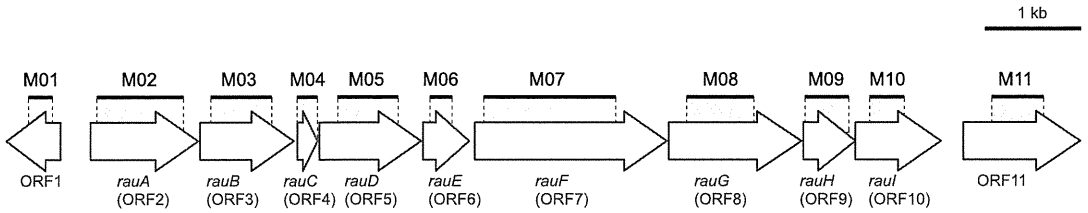

Table S1. Bacterial strains and plasmids used in this study

Strain or plasmid	Relevant characteristic(s)[a]	Reference or origin[b]
Strains		
Rhodococcus strains		
R. erythropolis JCM 6824	Wild type, aurachin RE producer, GI$^+$, antibiotic Group I (=strain R04)	JCM
R. erythropolis M18-8	Transposon mutant of JCM 6824, GI$^-$	This study
R. erythropolis M01	*orf1* mutant of strain JCM 6824, GI$^+$	This study
R. erythropolis M02	*rauA* (*orf2*) mutant of strain JCM 6824, GI$^-$	This study
R. erythropolis M03	*rauB* (*orf3*) mutant of strain JCM 6824, GI$^-$	This study
R. erythropolis M04	*rauC* (*orf4*) mutant of strain JCM 6824, GI$^-$	This study
R. erythropolis M05	*rauD* (*orf5*) mutant of strain JCM 6824, GI$^-$	This study
R. erythropolis M06	*rauE* (*orf6*) mutant of strain JCM 6824, GI$^-$	This study
R. erythropolis M07	*rauF* (*orf7*) mutant of strain JCM 6824, GI$^-$	This study
R. erythropolis M08	*rauG* (*orf8*) mutant of strain JCM 6824, GI$^\pm$	This study
R. erythropolis M09	*rauH* (*orf9*) mutant of strain JCM 6824, GI$^\pm$	This study
R. erythropolis M10	*rauI* (*orf10*) mutant of strain JCM 6824, GI$^+$	This study
R. erythropolis M11	*orf11* mutant of strain JCM 6824, GI$^+$	This study
R. erythropolis C02	M02 with pK4-rauA, GI$^+$	This study
R. erythropolis JCM 3201^T	Wild type, aurachin RE sensitive, Type strain	JCM
R. erythropolis pTipRQAI	JCM 3201 with pTipRQAI	This study
R. erythropolis pNitRQAI	JCM 3201 with pNitRQAI	This study
R. erythropolis M1218	Derivative strain of JCM 2895, non antibiotic producer	This study
Arthrobacter atrocyaneus JCM 1329^T	Wild type, aurachin RE sensitive	JCM

Table S1. Bacterial strains and plasmids used in this study (continued)

Strain or plasmid	Relevant characteristic(s)[a]	Reference or origin[b]
Plasmids		
pBluescriptII KS	Cloning vector, Ap^r	Stratagene
pTNR	Transposon mutagenesis vector (IS*1415*), Km^r	Sallam, et al, 2006
pK18mobsacB	Cloning vector, *mob*, *sacB*, Km^r	National institute of genomics, Japan
pK18M01	*orf1* disruption plasmid	This study
pK18M02	*orf2* disruption plasmid	This study
pK18M03	*orf3* disruption plasmid	This study
pK18M04	*orf4* disruption plasmid	This study
pK18M05	*orf5* disruption plasmid	This study
pK18M06	*orf6* disruption plasmid	This study
pK18M07	*orf7* disruption plasmid	This study
pK18M08	*orf8* disruption plasmid	This study
pK18M09	*orf9* disruption plasmid	This study
pK18M10	*orf10* disruption plasmid	This study
pK18M11	*orf11* disruption plasmid	This study
pK4	General cloning vector for *Rhodococcus* sp., Km^r	Hashimoto, et al., 1992
pK4-rauA	pK4 harboring *rauA*	This study
pTip-QC2	Expression vector for *Rhodococcus* sp., *tip* promoter (thiostrepton inducible), Cm^r, Ap^r	Nakashima and Tamura, 2004
pNit-QC2	Expression vector for *Rhodococcus* sp., *nit* promoter (constitutive), Cm^r, Ap^r	Nakashima and Tamura, 2004
pNit-rauA	pNitQC2 harboring *rauA*	This study
pTipRQAI	pTipQC2 harboring *rauA–I*	This study
pNitRQAI	pNitQC2 harboring *rauA–I*	This study
pET26b	Expression vector for *E. coli*	Novagen
pET-rauA-His	pET26b harboring *rauA* with C-terminus histidine tag sequence	This study

[a] GI^+, growth inhibition activity positive (against *Arthrobacter* strain); GI^-, growth inhibition activity negative; $GI^{\pm}$, weak growth inhibition activity; Ap^r, ampicillin resistance; Cm^r, chloramphenicol resistance; Km^r, kanamycin resistance.

[b] JCM, Japan Collection of Microorganisms; DSM, Deutsche Sammlung von Mikroorganismen und Zellkulturen GmbH; NBRC, NITE Biological Resource Center.

Table S2. Primers used in this study

Primer	Usage	Sequence (5′–3′)
ORF1-1F	Construction of pK18M01	ATGAAGCTTGACTGCGACTCACGCTTGC
ORF1-1R	Construction of pK18M01	ACGCTGCAGTCGACAGTGACGATATGGCC
ORF1-2F	Construction of pK18M01	CGACTGCAGTGATACGAGCAACCGTAACC
ORF1-2R	Construction of pK18M01	ATCTCTAGACGTGACTGAGAATGTGTCTCC
ORF2-1F	Construction of pK18M02	GTATAGAAGTCACCGTTCGAGC
ORF2-1R	Construction of pK18M02	GCAGGATCCGTAGTCAGCAACGATCCAGG
ORF2-2F	Construction of pK18M02	GACACATTCTCAGTCACGCG
ORF2-2R	Construction of pK18M02	CGCCTGCAGCTCATCGTCAATCGTCATGG
ORF3-1F	Construction of pK18M03	TGGGAATTCACATGCCACCATTCCTTGG
ORF3-1R	Construction of pK18M03	GTTCTCGAGTTCTACGGAGACGCAGAACG
ORF3-2F	Construction of pK18M03	GCGCTCGAGGCGTCATTCTCGGTGTACG
ORF3-2R	Construction of pK18M03	GTCCTGCAGGCGAACCATGTCATCATCG
ORF4-1F	Construction of pK18M04	GAGTCTAGAGACACATTCTCAGTCACGCG
ORF4-1R	Construction of pK18M04	CGCCTCGAGCTCATCGTCAATCGTCATGG
ORF4-2F	Construction of pK18M04	TGCCTCGAGTGCAGCAACTGATCCAATCC
ORF4-2R	Construction of pK18M04	AGTAAGCTTAGGTAATTCGCACACAGACG
ORF5-1F	Construction of pK18M05	TGGTCTAGACGACTGGTAGATCTTCCCGC
ORF5-1R	Construction of pK18M05	ACACTCGAGCTACAGGCCGATTACGTTCC
ORF5-2F	Construction of pK18M05	CTACTCGAGACGACCGAATATTCTCCGC
ORF5-2R	Construction of pK18M05	CGGAAGCTTTACGGCTATCCGGTGTTGC
ORF6-1F	Construction of pK18M06	ATCTCTAGATCTCTTCGCTCGATCTAATCG
ORF6-1R	Construction of pK18M06	AGTCTCGAGAGGTAATTCGCACACAGACG
ORF6-2F	Construction of pK18M06	GGTCTCGAGCCAATGGCATTCTGGCTTAC
ORF6-2R	Construction of pK18M06	ACTAAGCTTCGTGTTCTGTTGGAGGTGTG
ORF7-1F	Construction of pK18M07	AGGGAATTCGTGTTGTCGTCGTTGAACCC
ORF7-1R	Construction of pK18M07	CTGCTCGAGTTTCACGTTCACACTCGTCG
ORF7-2F	Construction of pK18M07	CTTCTCGAGTTGACTCGACTCTGGTTGTCC
ORF7-2R	Construction of pK18M07	ATTCTGCAGGAAGATCCATTGCCAACTCC
ORF8-1F	Construction of pK18M08	GCCTCGAATTCCTCTCACC
ORF8-1R	Construction of pK18M08	ATCCTCGAGCGCATACTCCGAAGAAGAGC
ORF8-2F	Construction of pK18M08	TACCTCGAGATCATCAACGGTCTCGATCC
ORF8-2R	Construction of pK18M08	ATCAAGCTTCATTGCCTATCTCCTTGCG
ORF9-1F	Construction of pK18M09	CGGTCTAGAGCTCTTCTTCGGAGTATGCG
ORF9-1R	Construction of pK18M09	TGTAGATCTGAAGTTTGTCCACGATTCCC
ORF9-2F	Construction of pK18M09	TTGAGATCTGACTGTGCTGGATACCCTCC
ORF9-2R	Construction of pK18M09	AATAAGCTTAAGTATCGTACCCGTCAATGG
ORF10-1F	Construction of pK18M10	ACTTCTAGACCTGGGCCTCTTTCGTAACC
ORF10-1R	Construction of pK18M10	GCAGCAAACCGAAGAGATGC
ORF10-2F	Construction of pK18M10	CAAGCGGCCGCGATATTCCGTCTTCCTCCC
ORF10-2R	Construction of pK18M10	CCCAAGCTTGACAGATTGACGAATGCTGC
ORF11-1F	Construction of pK18M11	AGGTCTAGACGAGAGATGATCATCGGGC
ORF11-1R	Construction of pK18M11	ATACTGCAGCGTATCTCGTCGGTGAGTGC
ORF11-2F	Construction of pK18M11	ACACTGCAGCCGATTCTTGGCACTCTTGC
ORF11-2R	Construction of pK18M11	AGCAAGCTTCTCAGCTACAAGCCGACGC

Table S2. Primers used in this study (continued)

Primer	Usage	Sequence (5′–3′)
aphII-UR	Single crossover detection, hybridize to kanamycin resistant gene (*aphII*)	ATCCATCTTGTTCAATCATGCG
ORF1-Single-C	*orf1* single crossover detection	CTCTGCAACTTCGATGGAGC
ORF2-Single-C	*orf2* single crossover detection	ACTATCCTGACCAGCAATGCC
ORF3-Single-C	*orf3* single crossover detection	AAGCAGATTATTCGGCAAGG
ORF4-Single-C	*orf4* single crossover detection	AGGACTGCGAGGTAAGTGGC
ORF5-Single-C	*orf5* single crossover detection	TAAGCCGATAGCAATGTCCG
ORF6-Single-C	*orf6* single crossover detection	CATGACGATTGACGATGAGC
ORF7-Single-C	*orf7* single crossover detection	GAATCGGATCAGGCTGTGC
ORF8-Single-C	*orf8* single crossover detection	TCGATTCCCACTTGGTTCC
ORF9-Single-C	*orf9* single crossover detection	CTGCAATGGATACTCGACTCC
ORF10-Single-C	*orf10* single crossover detection	GTCGTGATGCAACGACAGC
ORF11-Single-C	*orf11* single crossover detection	CAATGCTCGTTCTCGAAGG
ORF1-DCC-F	*orf1* double crossover detection	GCCTGAAGAAATCTTCGTTCC
ORF1-DCC-R	*orf1* double crossover detection	GAAGAAGATGACCATGAAGCG
ORF2-DCC-F	*orf2* double crossover detection	CTCGGGACTTTGGTCCTAGC
ORF2-DCC-R	*orf2* double crossover detection	TTCTACGGAGACGCAGAACG
ORF3-DCC-F	*orf3* double crossover detection	GAGGACTGCGAGGTAAGTGG
ORF3-DCC-R	*orf3* double crossover detection	CTCATCGTCAATCGTCATGG
ORF4-DCC-F	*orf4* double crossover detection	GGACTGTCCGTATTTCTCGC
ORF4-DCC-R	*orf4* double crossover detection	AATCACGTCGACATGTCCG
ORF5-DCC-F	*orf5* double crossover detection	TCTCTTCGCTCGATCTAATCG
ORF5-DCC-R	*orf5* double crossover detection	AGGTAATTCGCACACAGACG
ORF6-DCC-F	*orf6* double crossover detection	ACGACCGAATATTCTCCGC
ORF6-DCC-R	*orf6* double crossover detection	CTGTGGGCAATGACCATAGC
ORF7-DCC-F	*orf7* double crossover detection	GTGTTGTCGACACGTCTGG
ORF7-DCC-R	*orf7* double crossover detection	GACATCAGCATGTGCTCGG
ORF8-DCC-F	*orf8* double crossover detection	ACCTACTCCTGCCATGAAGG
ORF8-DCC-R	*orf8* double crossover detection	TGTCCAAATCAGGCTCAAGC
ORF9-DCC-F	*orf9* double crossover detection	GACATCGATCAAATGCAGGC
ORF9-DCC-R	*orf9* double crossover detection	GATCATCTCTCGTCGCATCC
ORF10-DCC-F	*orf10* double crossover detection	ATTGCAGCAGGAACTGAACG
ORF10-DCC-R	*orf10* double crossover detection	AGAGGTGGAGAATTCCGCG
ORF11-DCC-F	*orf11* double crossover detection	TTCCCGAAACCAAAGTTCG
ORF11-DCC-R	*orf11* double crossover detection	AGATCAGGGATGTTTGAGCC
rauA-F-NdeI	*rauA* cloning	GGACATATGACACACACGGTCGACG
rauA-R-HindIII	*rauA* cloning	GCGAAGCTTACATTGCTATCGGCTTACCG
rauA-XhoI-His-R	*rauA* cloning	ACACTCGAGTCGGCTTACCGCTACGGAAAG
rauA-F	Amplify partial *rauA*, for probe	ATACATCGCTCAGCTCTGGG
rauA-R	Amplify partial *rauA*, for probe	TCGACTGCTTCTCGATTTCC

ChemPubSoc Europe

DOI: 10.1002/cbic.201300386

A Single Mutation at the Ferredoxin Binding Site of P450 Vdh Enables Efficient Biocatalytic Production of 25-Hydroxyvitamin D_3

Yoshiaki Yasutake,[a] Taiki Nishioka,[b, c] Noriko Imoto,[b, d] and Tomohiro Tamura*[a, b]

Vitamin D_3 hydroxylase (Vdh) from *Pseudonocardia autotrophica* is a cytochrome P450 monooxygenase that catalyzes the two-step hydroxylation of vitamin D_3 (VD_3) to produce 25-hydroxyvitamin D_3 ($25(OH)VD_3$) and 1α,25-dihydroxyvitamin D_3 ($1\alpha,25(OH)_2VD_3$). These hydroxylated forms of VD_3 are useful as pharmaceuticals for the treatment of conditions associated with VD_3 deficiency and VD_3 metabolic disorder. Herein, we describe the creation of a highly active T107A mutant of Vdh by engineering the putative ferredoxin-binding site. Crystallographic and kinetic analyses indicate that the T107A mutation results in conformational change from an open to a closed state, thereby increasing the binding affinity with ferredoxin. We also report the efficient biocatalytic synthesis of $25(OH)VD_3$, a promising intermediate for the synthesis of various hydroxylated VD_3 derivatives, by using nisin-treated *Rhodococcus erythropolis* cells containing Vdh_{T107A}. The gene-expression cassette encoding *Bacillus megaterium* glucose dehydrogenase-IV was inserted into the *R. erythropolis* chromosome and expressed to avoid exhaustion of NADH in a cytoplasm during bioconversion. As a result, approximately 573 μg mL^{-1} $25(OH)VD_3$ was successfully produced by a 2 h bioconversion.

Introduction

Microbial processing is more efficient and friendly to the environment than chemical synthesis, because of its specificity and minimal use of organic solvents. Cytochrome P450 monooxygenases (P450s) are of special interest for the production of fine chemicals and pharmaceuticals because of their ability to insert oxygen into the nonactivated C–H bonds of various compounds, in a regio- and stereoselective manner and under mild conditions.[1] Generally, selective C–H bond oxygenation is one of the most challenging processes in synthetic chemistry; therefore, P450s are attractive candidates as biocatalysts in biotechnological applications.[2] P450s are heme-containing enzymes that use molecular oxygen and two-electron transfer from a hydride donor NAD(P)H via appropriate redox partner proteins (e.g., ferredoxin (Fdx) and ferredoxin reductase (FdxR)) for catalytic reactions.[3] They are involved in many physiological roles, including the biosynthesis of steroids, fatty acids, and complex antibiotics, and biological processes such as lipid homeostasis, detoxifying xenobiotics, and drug metabolism.[4–7]

Vitamin D_3 (VD_3) is a secosteroid, which is similar in structure to a steroid but has an opened B-ring. In humans, VD_3 is obtained from the diet or is synthesized from 7-dehydrocholesterol within the skin in response to sunlight. VD_3 is further converted into the active forms of VD_3, 25-hydroxyvitamin D_3 ($25(OH)VD_3$), in the liver, and then to 1α,25-dihydroxyvitamin D_3 ($1\alpha,25(OH)_2VD_3$) in the kidney. Both steps are catalyzed by several P450s.[8–11] The active forms of VD_3 regulate calcium homeostasis through interactions with VD_3 receptors in major tissues, bone, and the intestine. Thus, VD_3 metabolic disorders lead to low serum calcium levels (hypocalcemia) and defective mineralization of the bone matrix. Moreover, active forms of VD_3 function as hormones and play critical roles in controlling differentiation and proliferation of multiple cell types. Hydroxylated VD_3 and its derivatives are currently used as pharmaceuticals for the treating the symptoms of numerous disorders, such as rickets, osteomalacia, osteoporosis, hypoparathyroidism, and psoriasis.[12] Although chemical synthesis of $1\alpha,25(OH)_2VD_3$ from cholesterol is an established method, it is inefficient (yield $\leq$1%).[13] In contrast, microbial conversion using actinomycete *Pseudonocardia autotrophica* cells is practical for the production of $25(OH)VD_3$ and $1\alpha,25(OH)_2VD_3$.[14,15] *P. autotrophica* possesses P450 Vdh (CYP107BR1), a cytochrome P450 monooxygenase that hydroxylates VD_3. However, this microbial conversion requires a long reaction time (72 h for the production of 137 μg mL^{-1} $25(OH)VD_3$ under optimized culture conditions).[15]

[a] *Dr. Y. Yasutake,[+] Prof. T. Tamura*
Bioproduction Research Institute
National Institute of Advanced Industrial Science and Technology (AIST)
2-17-2-1, Tsukisamu-higashi, Toyohira-ku, Sapporo 062-8517 (Japan)
E-mail: t-tamura@aist.go.jp

[b] *Dr. T. Nishioka,[+] Dr. N. Imoto, Prof. T. Tamura*
Graduate School of Agriculture, Hokkaido University
Kita-9, Nishi-9, Kita-ku, Sapporo 060-8589 (Japan)

[c] *Dr. T. Nishioka[+]*
Current address: MicroBiopharm Japan, Co. Ltd.
1808 Nakaizumi, Iwata, Shizuoka 438-0078 (Japan)

[d] *Dr. N. Imoto*
Current address:
Department of Human Health Science,Hachinohe Gakuin University
13–98 Mihono, Hachinohe, Aomori 031-8588 (Japan)

[+] *These authors contributed equally to this work.*

Supporting information for this article is available on the WWW under http://dx.doi.org/10.1002/cbic.201300386.

To develop a more efficient method for the hydroxylation of VD_3, we have used a recombinant system by using *Rhodococcus erythropolis* cells.[16] There are three problems to overcome: permeability of VD_3 across the cell membrane is limited;[17] the catalytic activity of Vdh is relatively low because VD_3 is probably a nonnative substrate for Vdh; and, sufficient electrons are needed for the catalytic turnover of P450. To address the first issue (permeability), we recently developed a technique in which pore structures in the *Rhodococcus* cell membrane are generated by a small antimicrobial peptide (nisin) to improve the permeability of VD_3 into the cytoplasm.[18] For the second issue (catalytic activity), we constructed a quadruple mutant of Vdh (Vdh-K1: T70R/V156L/E216M/E384R) by directed evolution.[16] Unfortunately, the expression level of Vdh-K1 was very low in *R. erythropolis* cells, and, thus, was not suitable for *R. erythropolis* bioconversion. To date, several research groups have attempted to increase the productivity of active forms of VD_3. Fujii et al. reported 2.2-fold more efficient VD_3 bioconversion with *Escherichia coli*, by disruption of efflux pump genes (*AcrAB/TolC*).[19] Hayashi and co-workers reported bioconversion from VD_3 to several species of hydroxylated VD_3 metabolites by using a *Streptomyces* strain expressing CYP105A1.[20–22] Nevertheless, a dramatic improvement in the production of hydroxylated VD_3 has not been realized.

Herein, we report the creation of a highly active single mutant of Vdh (Vdh_{T107A}) by engineering the putative Fdx-binding site. Vdh_{T107A} was well expressed as an active heme-containing form in *R. erythropolis* cells. In addition, the gene encoding *Bacillus megaterium* glucose dehydrogenase was inserted into the chromosome of *R. erythropolis* JCM3201 and was expressed to provide a stable supply of NADH. Electrons were thus donated to Vdh from NADH by coexpressing the redox partner proteins, AciB (Fdx) and AciC (FdxR). Partially methylated β-cyclodextrin (PMβCD) was used to reduce 25(OH)VD_3 1α-hydroxylation activity,[15] as well as to increase the water solubility of VD_3. As a result, an exceptionally high yield of 25(OH)VD_3 (a promising intermediate for the synthesis of various hydroxylated VD_3 derivatives)[23] was achieved by using nisin-treated *R. erythropolis* cells.

Results and Discussion

Selection of redox partner proteins coupled with Vdh

Most bacterial P450s require two electrons sequentially delivered from NAD(P)H via redox partner proteins (e.g., FAD-containing FdxR, and the small iron–sulfur protein Fdx). Unfortunately, the native redox partner proteins for Vdh in *P. autotrophica* cells remain unknown. To select appropriate redox partner proteins for VD_3 bioconversion by *R. erythropolis* cells, we tested seven pairs of recombinant Fdx/FdxR proteins from *R. erythropolis* JCM3201. However, no useful redox partners were found. Therefore, we used AciB (Fdx) and AciC (FdxR) proteins from *Acinetobacter* sp. OC4[24] as redox partner proteins for Vdh. We have previously reported that AciB/AciC can reasonably be coupled with Vdh, both in vivo and in vitro.[18]

Site-directed mutagenesis at the Fdx binding site of Vdh

Generally, the combination of native P450 and Fdx showed a high electron-transfer rate from Fdx to P450 and, consequently, catalytic efficiency.[25] If the native redox partner for a particular P450 is unknown, site-directed mutagenesis of the putative Fdx/P450 association site is an attractive strategy for increasing P450s catalytic activity.[26–28] Therefore, in order to improve the VD_3 hydroxylating activity of Vdh, the amino-acid residues at putative Fdx-binding sites of Vdh were substituted with those from P450 AciA (CYP153A), an enzyme naturally coupled with AciB in *Acinetobacter* sp. OC4.[24] As the X-ray structure of P450 AciA has not been reported, the amino-acid residues involved in Fdx binding were identified based on the X-ray structure of P450cam from *Pseudomonas putida* (PDB ID: 2CPP; the best-characterized P450, including the intermolecular interactions with putidaredoxin (Fdx) by X-ray and NMR analyses,[29–33] site-directed mutagenesis,[34] and molecular docking simulations).[35,36] In total, eight residues were selected for mutational analysis; the corresponding residues of AciA were identified by sequence alignment in CLUSTALW[37] (Figures S1 and S2 in the Supporting Information). The mutants created and the VD_3 25-hydroxylase activities for these mutants are summarized in Table 1. VD_3 25-hydroxylase activity with mutations T107A, H342F, F346R, or Q351R was elevated compared to wild-type (Vdh_{WT}); two mutants (F106V and L348M) showed no catalytic activity. Interestingly, Vdh_{T107A} exhibited exceptionally high VD_3 25-hydroxylating activity (~80 times higher than Vdh_{WT}). This activity level is comparable to that of Vdh-K1, a quadruple Vdh mutant generated by directed evolution.[16]

Table 1. Comparison of specific activities of Vdh_{WT} and mutants against VD_3.

Variant	VD_3 25-hydroxylase activity [mol min^{-1} per mol of P450]	Relative activity
Vdh_{WT}	0.07 ± 0.01	1.0
Vdh-K1 (T70R/V156L/E216M/E384R)	5.42 ± 0.45	77.4
T96D	0.03 ± 0.01	0.5
F106V	n.d.	
T107A	5.54 ± 0.56	79.2
V108P	0.05 ± 0.00	0.7
F346R	0.08 ± 0.01	1.2
Q351R	0.15 ± 0.02	2.2
H342F	0.10 ± 0.01	1.4
L348M	n.d.	

n.d.: not detected.

Kinetic analysis

To evaluate kinetic parameters describing the enzymatic changes, we performed a reconstituted in vitro enzyme assay, and measured VD_3 25-hydroxylase activity with varying concentration of AciB; K_m and k_{cat} were calculated by fitting Mi-

Table 2. Kinetic parameters for AciB on VD_3 25-hydroxylation activity.

	K_m [μM]	k_{cat} [min^{-1}]	k_{cat}/K_m [min^{-1} M^{-1}]
Vdh_{WT}	85.7 ± 8.4	0.81 ± 0.18	9.45×10^3
Vdh_{T107A}	24.5 ± 3.8	23.0 ± 1.40	9.39×10^5
Vdh-K1	19.7 ± 4.1	20.8 ± 1.37	1.06×10^6

chaelis–Menten plots for Vdh_{WT}, Vdh-K1, and Vdh_{T107A} (Table 2). The results show that k_{cat} increased from 0.81 to 23.0 min^{-1}, and K_m decreased from 85.7 to 24.5 μM, for the single mutation T107A. Interestingly, Vdh-K1 exhibited similar kinetic properties to Vdh_{T107A}. These results indicate that the four mutations of Vdh-K1 and the single mutation of Vdh_{T107A} lead to similar changes in the enzymatic properties related to the enhancement of the binding affinity to AciB (Table 2).

VD_3 25-hydroxylation activity was also measured with commercially available spinach Fdx/FdxR, which is commonly used as a redox partner protein pair for in vitro reconstituted P450 assays. The results showed that the VD_3 25-hydroxylation activity of both Vdh-K1 and Vdh_{T107A} increased ~50-fold (Table S1), similar to the results obtained with AciB/AicC. This suggests that the T107A mutation and the four mutations of Vdh-K1 do not contribute to improvement in AciB specificity, but affect the underlying catalytic mechanism of Vdh and thus bring about high catalytic efficiency. A single mutation at the molecular surface might seem trivial; however, the T107A mutation confers upon Vdh the ability to function at a level approximate equivalent to that of Vdh-K1. Our previous structural and spectroscopic studies indicated that the conformational change from an open to a closed state (resulting from the four mutations in Vdh-K1) led to a dramatic increase in catalytic activity.[38] Therefore, it would be of great interest to determine the structure of Vdh_{T107A}. Investigations should determine whether it is possible to change the conformation of Vdh by just removing the hydroxyl and methyl groups of Thr107.

Crystal structure of Vdh_{T107A} exhibits a closed conformation

Crystals of Vdh_{T107A} with different morphology can be obtained from different crystallization solutions, and compared to those of Vdh_{WT} and Vdh-K1. The crystallization conditions used for Vdh_{WT} and Vdh-K1 did not yield crystals of Vdh_{T107A}. The structure of Vdh_{T107A} in a complex with VD_3 was solved at a resolution of 2.57 Å by molecular replacement. The asymmetric unit comprises a single monomer (Matthews coefficient, V_m = 2.53 $Å^3 Da^{-1}$). The final refined model consists of amino acid residues 2 to 403, the heme cofactor, VD_3, and 36 water molecules, with crystallographic R and R_{free} factors of 0.187 and 0.231, respectively (crystallographic parameters and refinement statistics are summarized in Table 3). The electron density was of high quality, thus allowing good definition of the model, with the exception of the C-terminal His tag region.

The structure of Vdh_{T107A} was superimposed onto that of Vdh-K1 (which forms a closed conformation) with a root mean square deviation (RMSD) of 0.7 Å for 390 Cα atoms (Figures 1 and S3, and Movie S1). The results clearly show that Vdh_{T107A} exhibits a closed conformation similar to that of Vdh-K1 bound to VD_3. Main-chain and side-chain conformations at the active-site region of Vdh_{T107A} superimposed well onto those of Vdh-K1 (Figure S5). The closed conformation of Vdh can be characterized by the ~8 Å shift of the helices F/G and the local conformational change around the HI-loop (nomenclature of the secondary structure elements follows the established convention).[38] In the structure of Vdh_{T107A}, Asp219 in the HI-loop contacts neighboring monomers in the crystal lattice; no crystal contacts were found in the vicinity of helices F/G, which directly cover the substrate-binding site and separate it from the solvent. Therefore, we assume that the current closed form of Vdh_{T107A} is not a crystallization artifact but reflects the conformational state in solution. P450 is generally considered exhibit conformational dynamics (between open and closed states) in solution,[39–42] and, thus, similarly to Vdh-K1, the T107A mutation might be responsible for the shift in the conformational equilibrium towards the closed state. Molecular dynamic simulation is currently underway to demonstrate how the mutation affects the conformational dynamics of Vdh.

It is known that, in general, the P450-binding surface of Fdx is negatively charged and the Fdx-binding surface of P450 is positively charged. These opposite electrostatic characteristics of the molecular surfaces are known to be responsible for the association between P450 and Fdx.[35,43,44] Kinetic studies have shown that the AciB-binding affinities of Vdh-K1 and Vdh_{T107A} were approximately threefold higher than that of Vdh_{WT}. We therefore calculated the electrostatic charge distributions for Vdh_{WT}, Vdh-K1, and Vdh_{T107A}. Evidently, the electrostatic charge potentials of the Fdx-binding surfaces of Vdh_{T107A} and Vdh-K1

Table 3. Crystallographic parameters and model refinement statistics of Vdh_{T107A}.

Data collection statistics	
beamline	BL-5A, PF
wavelength [Å]	1.0000
resolution [Å]	50–2.57 (2.64–2.57)[a]
unit cell dimensions	
a, *b*, *c* [Å]	61.4, 105.5, 142.0
space group	$C222_1$
unique reflections	14156
R_{sym}[b]	0.048 (0.557)[a]
completeness [%]	98.6 (92.3)[a]
redundancy	5.8 (5.6)
mean I/σ (I)	24.2 (3.1)[a]
Refinement statistics and model quality	
resolution range [Å]	50–2.57
R_{work}[c]	0.187
R_{free}[d]	0.231
total number of atoms	3212
average *B* factor [$Å^2$]	76.7
RMSD bond distances [Å]	0.008
RMSD bond angles [°]	1.93

[a] Values in parentheses refer to data in the highest resolution shell. [b] $R_{sym} = \Sigma_h \Sigma_i |I_{h,i} - \langle I_h \rangle| / \Sigma_h \Sigma_i I_{h,i}$, where $\langle I_h \rangle$ is the mean intensity of a set of equivalent reflections. [c] $R_{work} = \Sigma ||F_{obs}| - |F_{calcd}|| / \Sigma |F_{obs}|$ for 95% of the reflection data used in the refinement. F_{obs} and F_{calcd} are the observed and calculated structure factor amplitudes, respectively. [d] R_{free} is the equivalent of R_{work}, except that it was calculated for a randomly chosen 5% test set excluded from refinement.

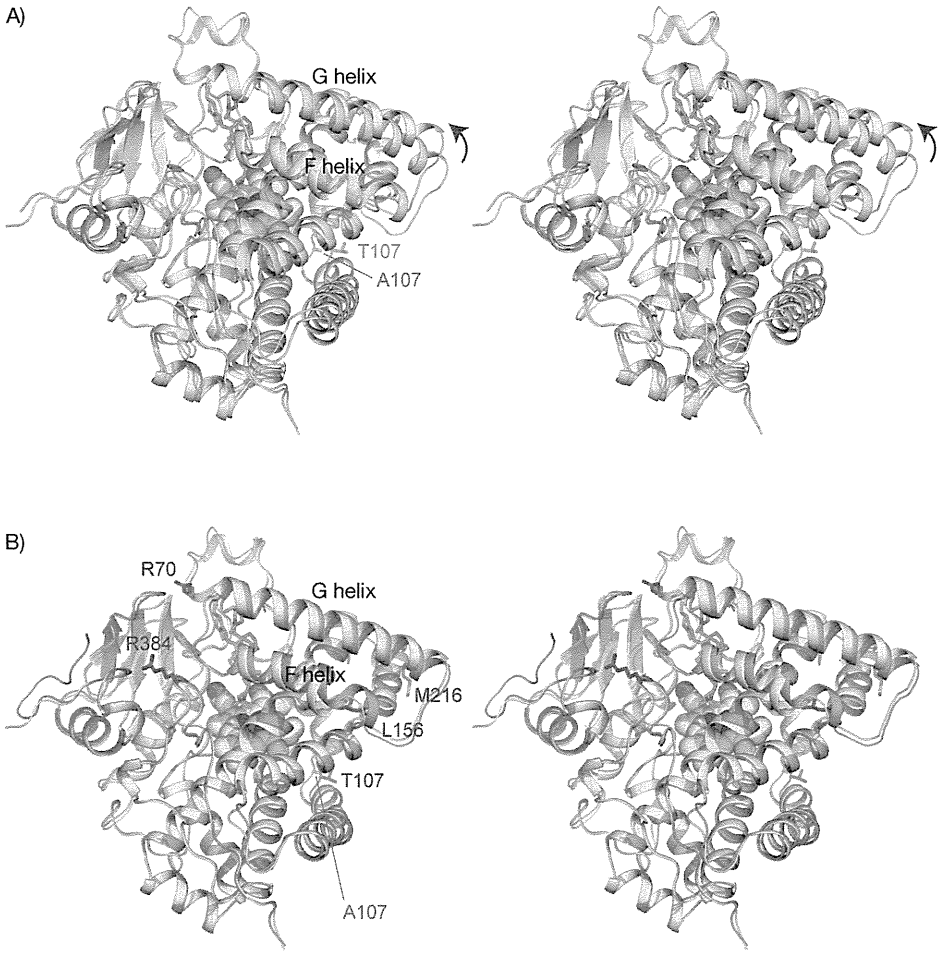

Figure 1. Stereoview superimpositions of X-ray structures of A) Vdh_{WT} (cyan, open conformation) and Vdh_{T107A} (yellow, closed conformation), and B) Vdh-K1 (purple, closed conformation) and Vdh_{T107A} (yellow, closed conformation). Side chains of the mutated residues in Vdh_{T107A}/Vdh-K1 are shown as sticks and labeled; mobile F- and G-helices are labeled; bound VD_3 is shown as sticks (green).

exhibit a more positively charged potential than that of Vdh_{WT}, thus indicating that the closed conformation could be more suitable for Fdx association (Figure 2). Although there are no remarkable changes in the overall structure of helices and loops of the Fdx-binding surface, subtle conformational changes in the CD helices are evident. In addition, there are significant alterations to the side-chain conformations of Arg110 (D-helix) and Arg220 (HI-loop; Figure 2). It is likely that these changes affect the electrostatic charge distribution on the Fdx-binding surface. We also found similar difference in electrostatic surface potential in P450 PikC (CYP107L1; PDB ID: 2BVJ), the P450 structure most homologous to Vdh.[39] Structures of substrate-free PikC have been solved in both open and closed conformations. Similarly to Vdh, the Fdx-binding surface of the closed form of PikC is more positively charged than that in open form (Figure S6). These observations indicate that the conformational change from an open to a closed state could be important for association with Fdx and substrate binding. Searching for mutation loci affecting conformational equilibrium is an interesting approach to identify useful mutants of a target P450 enzyme for improved activity.

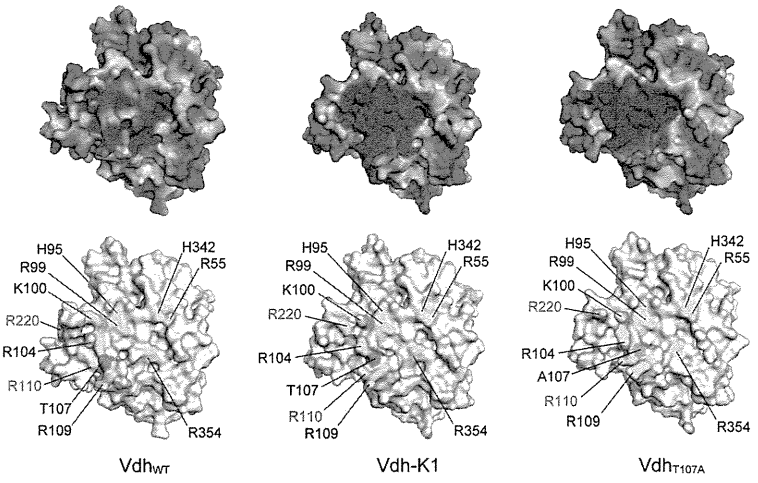

Figure 2. Electrostatic potentials of Fdx-binding surfaces of Vdh_{WT}, Vdh-K1, and Vdh_{T107A}. Potentials were calculated with the Adaptive Poisson–Boltzmann solver (APBS), and are presented in the range −4 (red) to +44 kT/e (blue). The same surface models showing the positions of basic residues and the mutated residue T107/A107 on the Fdx-binding surface are shown below. Arg220 and Arg110, which probably contribute to the change in electrostatic potential, are indicated in red (see text).

Bioconversion of VD_3 to 25(OH)VD_3 in nisin-treated *R. erythropolis* cells

Recently, we have developed a biocatalytic conversion system that uses nisin-treated *R. erythropolis* cells.[18] Nisin is a natural antimicrobial polypeptide and plays a role in increasing VD_3 permeability across the cell membrane (by forming a pore in the cell membrane). Previous studies demonstrated that nisin inhibits cell growth of actinomycetes by forming pores, thus leading to efflux of many vital intracellular compounds. However, proteins with relatively large molecular weight do not leak out, as the diameter of the nisin-forming pore is no more than 2.0–2.5 nm.[45,46] Importantly, nisin does not cause lysis of *R. erythropolis* cells, and, thus, nisin-treated dead *R. erythropolis* cells are useful as a biocatalytic system: overexpressed enzymes

for the bioconversion reaction are retained in the cytoplasm. In our previous study, VD_3 bioconversion to 25(OH)VD_3 was performed by using nisin-treated *R. erythropolis* JCM3201 cells that coexpressed Vdh_{WT} and redox partner proteins AciB and AciC.[18] NADH and *B. megaterium* glucose dehydrogenase IV (BmGlcDH-IV)[47,48] were added to the bioconversion solution to maintain a supply of NADH to P450. However, the Vdh-K1 mutant obtained by directed evolution could not be well expressed in *R. erythropolis* cells; thus, its performance was not suitable for this system. Indeed, the thermostability of Vdh-K1 was found to be lower than that of Vdh_{WT} and Vdh_{T107A} (Figure S7).

The activity of Vdh_{T107A} is comparable to that of Vdh-K1. The thermostability of Vdh_{T107A} is comparable to that of Vdh_{WT} (Figure S7), and Vdh_{T107A} can be reliably overexpressed in *R. erythropolis* cells: the expression level of Vdh_{T107A} is approximately 70% of that of Vdh_{WT}. Prior to the bioconversion test, we adapted *R. erythropolis* JCM3201 to incorporate the BmGlcDH-IV gene in its chromosome by a random transposon mutagenic system,[49] to maintain a supply of NADH within the cytoplasm. The resulting strain was termed JCM3201-GlcDH. A schematic diagram of the bioconversion is shown in Figure 3, and the results of the bioconversion are given in Figure 4. Bioconversion with nisin-treated *R. erythropolis* JCM3201-GlcDH containing Vdh_{T107A} was the most effective: almost 300 $\mu g\,mL^{-1}$ of 25(OH)VD_3 was produced after only 2 h of bioconversion (Figure 4A). We then performed repeated production of 25(OH)VD_3, based on previously described procedures.[18] The reaction solution (5 mL) was refreshed every 2 h, and four consecutive conversion reactions (total ca. 8 h) were carried out under optimized conditions (0.2 mM NADH, $OD_{600} = 10.0$). It is likely that iterative bioconversion reactions result in degradation or loss of biocatalyst (nisin-treated cells containing Vdh_{T107A} and other proteins) by harvesting and resuspension. However, the activity level was still approximately 60% after three cycles (Figure 4B), and the total amount of 25(OH)VD_3 obtained by this biocatalyst-reusing method was approximately 9 mg. Production of 25(OH)VD_3 in this and previously studies is summarized in Table 4.

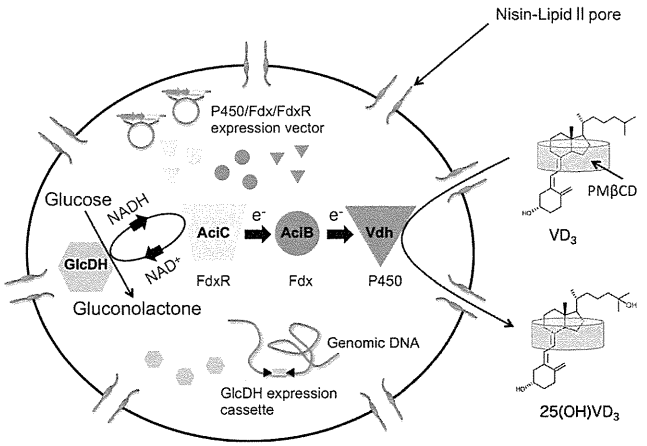

Figure 3. Nisin-treated *R. erythropolis* JCM3201-GlcDH bioconversion of VD_3 into 25(OH)VD_3. PMβCD was used to increase the solubility of VD_3/25(OH)VD_3, as well as to reduce second-step hydroxylation (see text). The pore in the cell membrane generated by nisin treatment afforded permeability of the PMβCD-VD_3 complex.

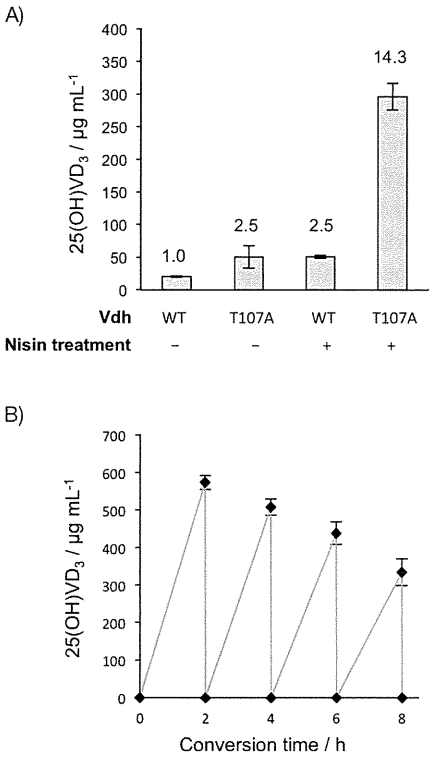

Figure 4. Biocatalytic production of 25(OH)VD_3 by nisin-treated *R. erythropolis* JCM3201-GlcDH cells containing Vdh_{T107A}. A) Effect of T107A mutation on bioconversion; the relative amounts of 25(OH)VD_3 production are shown. The combination of nisin treatment and Vdh_{T107A} resulted in an approximately 14-fold increase in bioconversion efficiency. B) Repeated biocatalytic production of 25(OH)VD_3 according to the same procedure but with reaction-buffer refreshment every 2 h. In this experiment, double the amount of cells was used compared to (A); see the Experimental Section. Error bars indicate standard deviation of three independent experiments.

Table 4. Bioconversion of VD_3 into 25(OH)VD_3 in this and previous studies.

Species	Enzyme	25(OH)VD_3 production [$\mu g\,mL^{-1}$]	Reaction time [h]	Ref.
P. autotrophica	Vdh_{WT}	137	48	[15]
E. coli	Vdh_{WT}	216	24	[19]
Streptomyces lividans	CYP105A1 (R73V/R84A)	7.8	24	[20]
R. erythropolis	Vdh_{WT}	342	16[a]	[18]
R. erythropolis	Vdh_{T107A}	573	2	this study

[a] This value (not given in the literature) was calculated from the raw data.

Conclusions

We obtained a highly active Vdh mutant (Vdh_{T107A}) by engineering the putative Fdx-binding site. In vitro reconstituted assay showed that Vdh_{T107A} was approximately 80 times more active than Vdh_{WT}. Kinetic analyses indicate that Vdh_{T107A} has

improved binding affinity with *Acinetobacter* Fdx (AciB), thereby improving VD_3 hydroxylation activity. The crystal structure of Vdh_{T107A} exhibited a closed conformation similar to that of Vdh-K1, a highly active quadruple mutant acquired by directed evolution. Similarly to Vdh-K1, it is likely that the T107A mutation is responsible for the shift in the conformational equilibrium in solution from the open to the closed state. The electrostatic surface distribution revealed that the Fdx-binding site of the closed conformation was more positively charged than that of the open conformation. These observations suggest that the closed form is more suitable for binding to negatively charged Fdx. Finally, we tested VD_3 bioconversion to $25(OH)VD_3$ by using nisin-treated *R. erythropolis* JCM3201-GlcDH (coexpressed Vdh_{T107}/AciB/AciC), and showed exceptionally high yield of $25(OH)VD_3$. VD_3 bioconversion by nisin-treated *R. erythropolis* JCM3201-GlcDH represents a simple strategy and application, and could be widely useful for P450-mediated conversion of other fat-soluble and/or toxic molecules for living cells coexpressing appropriate redox partner proteins.

Experimental Section

Materials: *R. erythropolis* JCM3201 (Japan Collection of Microorganisms), *E. coli* XL1-Blue, and *E. coli* BL21-CodonPlus(DE3)-RIL cells were routinely cultured in lysogeny broth (LB). Competent cells of *R. erythropolis* were prepared according to the procedure outlined by Shao et al.[50] Transformation of *R. erythropolis* JCM3201 was performed according to a previously described method.[51] Oligonucleotides were obtained from Hokkaido System Science (Sapporo, Japan). PCR was performed with *Pfu* Turbo DNA polymerase (Stratagene/Agilent) or KOD FX polymerase (Toyobo, Osaka, Japan). Restriction endonucleases were purchased from New England BioLabs and Promega. The DNA ligation kit was purchased from Takara Bio (Shiga, Japan). A Wizard SV Gel and PCR Clean-Up System (Promega) was used to purify PCR products from gel before cloning or sequencing. DNA was sequenced with a BigDye Terminator v3.1 Cycle Sequencing Kit (Applied Biosystems/Life Technologies) on an ABI Prism 3100 automated sequencer (Applied Biosystems) according to the manufacturer's instructions.

Overexpression and purification of recombinant protein for in vitro assay: Recombinant and mutant Vdh for the in vitro assay contained a C-terminal His_6 tag. Vdh mutants were prepared by inverse PCR[52] with synthetic oligonucleotide primers and pET29b-Vdh_{WT}[38] as the template. Recombinant Vdh_{WT} and mutants were produced in *E. coli* BL21 CodonPlus (DE3)-RIL, and purified as previously described.[38] A carbon monoxide difference spectra assay was performed to assess Vdh concentration.[53]

The gene encoding AciB from *Acinetobacter* sp. OC4 (Gene Bank accession: AB221118) was amplified by PCR with pTipQC2-Vdh-AciB-AciC as template DNA.[18] and inserted between the NdeI and XhoI sites of the pET28a expression vector. Transformed *E. coli* cells were grown at 37 °C in LB medium (100 mL), then overnight culture was inoculated into LB (900 mL). Expression was induced by addition of isopropyl-β-D-thiogalactoside (IPTG, 0.1 mM), and the cells were cultured overnight at 25 °C. Cells were harvested by centrifugation (2975 *g*, 10 min, 4 °C ?) and resuspended in buffer A (Tris·HCl (50 mM, pH 7.5), NaCl (100 mM), glycerol (10%)) containing lysozyme (1 mg mL^{-1}) and Benzonase (50 U mL^{-1}; Merck Millipore). The cells were disrupted by sonication, and the homogenate was clarified by centrifugation (39191 *g*, 10 min, 4 °C). The supernatant was loaded onto a Ni-affinity column (Sigma–Aldrich) equilibrated with buffer A, and then eluted with a linear gradient of imidazole (0–0.4 M in buffer A). The brown-colored fractions were pooled, and the concentrated sample was further purified on a Sephacryl S-100 size-exclusion column (2.5×90 cm; GE Healthcare). Finally, fractions were loaded onto a Q sepharose Fast Flow column (GE Healthcare) equilibrated with buffer A, and bound protein was eluted with a linear gradient of NaCl (0.1–0.6 M in buffer A). Purified AciB was dialyzed against Tris·HCl (25 mM, pH 7.5) with glycerol (20%) and stored at −20 °C. AciB concentration was estimated as previously described with minor modifications.[54] The sample in Tris·HCl (100 mM, pH 8.5) and SDS (2%) was denaturated by incubation for 15 min at 60 °C for, then further incubated with bathophenanthroline disulfonate (BPS, 0.2 mM) and dithionite (8 mM) for 30 min at 30 °C. The iron content of Fdx was determined by absorbance of the Fe^{2+}–BPS complex (ε_{535} = 25100 M^{-1} cm^{-1}).

The gene encoding *aciC* from *Acinetobacter* sp. OC4 (accession: AB221118) was amplified by PCR with pTipQC2-Vdh-AciB-AciC as template DNA,[18] and inserted between NdeI and XhoI sites of a pET26a expression vector (culture and induction as for AciB). The cells were harvested and resuspended in buffer B (sodium phosphate (50 mM, pH 8.0), NaCl (300 mM)) containing lysozyme (1 mg mL^{-1}) and Benzonase (~50 U mL^{-1}), and then disrupted by sonication. After centrifugation (39191 *g*, 10 min, 4 °C), the supernatant was loaded onto a Ni-affinity column (Sigma–Aldrich) equilibrated with buffer B. The column was washed with buffer C (sodium phosphate (50 mM, pH 6.0), NaCl (300 mM), glycerol (10%)) and eluted with a linear gradient of imidazole (0–0.4 M in buffer C). The yellow-colored fractions were pooled and dialyzed against buffer D (Tris·HCl (25 mM, pH 7.5, glycerol (10%)). The dialyzed sample was loaded onto a DEAE Sepharose Fast Flow Column (GE Healthcare) equilibrated with buffer D, and bound protein was eluted with a liner gradient of NaCl (0–0.6 M in buffer D). After boiling and removal of denatured protein, the concentration of flavin was calculated (ε_{473} = 9.2 mM^{-1} cm^{-1}).[55]

In vitro reconstitution assay and kinetic analysis: VD_3 25-hydroxylase activity of Vdh_{WT} and its mutants was measured by reconstitution experiments. The reaction mixture (200 μL) for enzyme activity measurements comprised Tris·HCl (50 mM, pH 7.5), NaCl (100 mM), AciB (10 μM) or spinach Fdx (100 μg mL^{-1}), AciC (1.0 μM) or spinach FdxR (0.1 U mL^{-1}), VD_3 (20 μM), NADH (200 μM; for AciB-AciC system) or NADPH (200 μm; for spinach system), and PMβCD (0.05%, *w/v*). The concentration of Vdh_{WT} (or mutant) was adjusted within the linear range of the assay. The reaction was initiated by addition of NADH/NADPH, and followed by incubation at 30 °C for 5 min. The reaction was stopped by addition of ethyl acetate (50 μL), and the mixture was extracted with ethyl acetate (800 μL). The product $25(OH)VD_3$ was detected by HPLC analysis as previously described.[18] The K_m and k_{cat} values for AciB were estimated from Michaelis–Menten plots (triplicate experiments) with titration of AciB (5–80 μM).

Crystallization and X-ray structure determination: Purified Vdh_{T107A} was concentrated to 20 mg mL^{-1}, and VD_3 was added (0.5 mM) for crystallization. All crystallization experiments were performed by the vapor-diffusion technique at 20 °C. An initial search for crystallization conditions was performed by using sparse matrix screen kits of Hampton Research (Aliso Viejo, CA) and Emerald Bio (Bedford, MA), and conditions were optimized by varying buffer pH and precipitant concentrations. Plate-shaped crystals (0.20×0.40×0.02 mm) grew in the solution containing Bis·Tris (0.1 M, pH 6.0–7.0), NaCl (0.2 M), and PEG 3350 (15–20%). X-ray diffraction

data were collected at beamline BL-5A of the Photon Factory (Tsukuba, Japan) with a Quantum 210r detector (ADSC Poway, CA). Prior to data collection, the crystal was soaked in cryoprotectant supplemented with glycerol (20%) and flash-cooled under a stream of nitrogen (100 K). The Vdh_{T107A} crystal belongs to the space group $C222_1$, with unit-cell dimensions $a=61.4$, $b=105.5$, $c=142.0$ Å. The diffraction data were processed by using the program XDS.[56] The structure of Vdh_{T107} was determined by the molecular replacement method by using the program MOLREP.[57] The X-ray model of Vdh-K1 (PDB ID: 3A50)[38] was used as a search model. The atomic coordinates and their *B*-factors were refined in REFMAC5,[58] and manual model corrections were performed with the graphic program COOT.[59] The stereochemical quality of the final refined model was checked by the program PROCHECK.[60] Crystallographic parameters and refinement statistics are summarized in Table 3. Molecular images were prepared with the program PyMOL (DeLano Scientific; http://pymol.org/). Electrostatic surface potentials were calculated by the Adaptive Poisson–Boltzmann Solver (APBS).[61]

Biocatalytic production of 25(OH)VD_3 by nisin-treated *R. erythropolis* cells: Expression vectors pTipQC2-Vdh_{WT}-AciB-AciC and pTipQC2-Vdh_{T107A}-AciB-AciC were constructed according to a previously described method.[18] The gene encoding BmGlcDH-IV was amplified by PCR with pET28a-BmGlcDH-IV as template DNA,[48] and was inserted between the NdeI and XhoI sites of the expression vector pNitQC2.[51] From this, a BmGlcDH-IV expression cassette (P_{nit} promoter, *BmGlcDH-IV* sequence, and T_{thcA} transcriptional terminator) was amplified by PCR, and inserted between the StuI and NsiI sites of the transposon-based expression vector to yield pTNR-KA-BmGlcDH-IV.[49] This was transformed into *R. erythropolis* JCM3201; the resulting strain was termed JCM3201-GlcDH. Expression of BmGlcDH-IV was confirmed by detecting GlcDH activity in the crude extract of the JCM3201-GlcDH, by monitoring NADH production (340 nm) in the presence of NAD^+ and D-glucose. JCM3201-GlcDH cells were transformed with pTipQC2-Vdh_{WT}-AciB-AciC or pTipQC2-Vdh_{T107A}-AciB-AciC, and grown in LB (20 mL) at 28 °C. Expression of Vdh_{WT}/Vdh_{T107A}, AciB, and AciC was induced by addition of thiostrepton (0.5 μg mL^{-1}) when cell growth reached the mid-log phase ($OD_{600}\approx0.7$). At 24 h after induction, cells were harvested by centrifugation (1940 *g*, 10 min, 4 °C), and the pellets were washed twice with potassium phosphate buffer (50 mM, pH 7.4), and resuspended ($OD_{600}=5.0$) in the same buffer (5 mL) supplemented with D-glucose (2%), glycerol (10%), VD_3 (2 mM), NADH (2 mM), PMβCD (1.5%), without or with nisin (0.5 mg mL^{-1}). After incubation with shaking (120 rpm, 2 h), the reaction mixture (50 μL) was added to methanol (450 μL) and gently mixed. The resulting solution was centrifuged (20817 *g*, 5 min, 20 °C), and the supernatant was analyzed by HPLC as previously described.[18] The repeated production (see text) was also performed with nisin-treated *R. erythropolis* JCM3201-GlcDH cells with pTipQC2-Vdh_{T107A}-AciB-AciC. The reaction buffer contained potassium phosphate (50 mM, pH 7.4), D-glucose (2%), glycerol (10%), VD_3 (2 mM), NADH (0.2 mM), PMβCD (1.5%), and nisin (0.5 mg mL^{-1}). We found that the bioconversion rate was roughly constant for NADH ≥ 0.2 mM, and thus the concentration of NADH was reduced to 0.2 mM in this experiment (bioconversion mixture $OD_{600}=10.0$). The buffer was changed every 2 h, and four consecutive reactions (total, 8 h) were performed. The reaction product was analyzed by HPLC as previously described.[38]

Accession number: The atomic coordinates and structure details have been deposited in the Protein Data Bank, http://www.pdb.org under PDB ID 3VRM.

Acknowledgements

The authors would like to thank Risa Yamagata for technical support. We also thank Dr. Akira Arisawa of MicroBiopharm Japan Co., Ltd. for the kind gift of the aciB/aciC genes. We are grateful to the beamline scientists at the Photon Factory (Tsukuba, Japan) for their kind assistance with X-ray diffraction experiments. This work was supported in part by the Development of Basic Technologies for Advanced Production Methods Using Microorganism Functions project of the New Energy and Industrial Technology Development Organization (NEDO) of Japan. This work was also supported in part by a Grant-in-Aid for Scientific Research from the Japan Society for the Promotion of Sciences (JSPS). Synchrotron radiation experiments were conducted under the approvals of 2011G129 at the Photon Factory.

Keywords: biosynthesis · crystal growth · cytochrome P450 · nisin · *Rhodococcus erythropolis* · vitamin D_3

[1] P. R. Ortiz de Montellano, *Chem. Rev.* **2010**, *110*, 932–948.
[2] M. K. Julsing, S. Cornelissen, B. Bühler, A. Schmid, *Curr. Opin. Chem. Biol.* **2008**, *12*, 177–186.
[3] F. Hannemann, A. Bichet, K. M. Ewen, R. Bernhardt, *Biochim. Biophys. Acta Gen. Subj.* **2007**, *1770*, 330–344.
[4] A. Chefson, K. Auclair, *Mol. BioSyst.* **2006**, *2*, 462–469.
[5] R. Bernhardt, *J. Biotechnol.* **2006**, *124*, 128–145.
[6] V. B. Urlacher, M. Girhard, *Trends Biotechnol.* **2012**, *30*, 26–36.
[7] C. J. C. Whitehouse, S. G. Bell, L.-L. Wong, *Chem. Soc. Rev.* **2012**, *41*, 1218–1260.
[8] D. E. Prosser, G. Jones, *Trends Biochem. Sci.* **2004**, *29*, 664–673.
[9] N. Sawada, T. Sakaki, M. Ohta, K. Inouye, *Biochem. Biophys. Res. Commun.* **2000**, *273*, 977–984.
[10] N. Strushkevich, S. A. Usanov, A. N. Plotnikov, G. Jones, H.-W. Park, *J. Mol. Biol.* **2008**, *380*, 95–106.
[11] K. Yamamoto, E. Uchida, N. Urushino, T. Sakaki, N. Kagawa, N. Sawada, M. Kamakura, S. Kato, K. Inouye, S. Yamada, *J. Biol. Chem.* **2005**, *280*, 30511–30516.
[12] G. Jones, S. A. Strugnell, H. F. DeLuca, *Physiol. Rev.* **1998**, *78*, 1193–1231.
[13] G.-D. Zhu, W. H. Okamura, *Chem. Rev.* **1995**, *95*, 1877–1952.
[14] J. Sasaki, A. Miyazaki, M. Saito, T. Adachi, K. Mizoue, K. Hanada, S. Omura, *Appl. Microbiol. Biotechnol.* **1992**, *38*, 152–157.
[15] K. Takeda, T. Asou, A. Matsuda, K. Kimura, K. Okamura, R. Okamoto, J. Sasaki, T. Adachi, S. Omura, *J. Ferment. Bioeng.* **1994**, *78*, 380–382.
[16] Y. Fujii, H. Kabumoto, K. Nishimura, T. Fujii, S. Yanai, K. Takeda, N. Tamura, A. Arisawa, T. Tamura, *Biochem. Biophys. Res. Commun.* **2009**, *385*, 170–175.
[17] J. Sikkema, J. A. M. de Bont, B. Poolman, *Microbiol. Rev.* **1995**, *59*, 201–222.
[18] N. Imoto, T. Nishioka, T. Tamura, *Biochem. Biophys. Res. Commun.* **2011**, *405*, 393–398.
[19] T. Fujii, Y. Fujii, K. Machida, A. Ochiai, M. Ito, *Biosci. Biotechnol. Biochem.* **2009**, *73*, 805–810.
[20] K. Hayashi, K. Yasuda, H. Sugimoto, S. Ikushiro, M. Kamakura, A. Kittaka, R. L. Horst, T. C. Chen, M. Ohta, Y. Shiro, T. Sakaki, *FEBS J.* **2010**, *277*, 3999–4009.
[21] K. Hayashi, H. Sugimoto, R. Shinkyo, M. Yamada, S. Ikeda, S. Ikushiro, M. Kamakura, Y. Shiro, T. Sakaki, *Biochemistry* **2008**, *47*, 11964–11972.
[22] T. Sakaki, H. Sugimoto, K. Hayashi, K. Yasuda, E. Munetsuna, M. Kamakura, S. Ikushiro, Y. Shiro, *Biochim. Biophys. Acta Proteins Proteomics* **2011**, *1814*, 249–256.
[23] A. Toyoda, H. Nagai, T. Yamada, Y. Moriguchi, J. Abe, T. Tsuchida, K. Nagasawa, *Tetrahedron* **2009**, *65*, 10002–10008.
[24] T. Fujii, T. Narikawa, F. Sumisa, A. Arisawa, K. Takeda, J. Kato, *Biosci. Biotechnol. Biochem.* **2006**, *70*, 1379–1385.

[25] S. G. Bell, F. Xu, E. O. D. Johnson, I. M. Forward, M. Bartlam, Z. Rao, L.-L. Wong, *J. Biol. Inorg. Chem.* **2010**, *15*, 315–328.
[26] L. S. Koo, C. E. Immoos, M. S. Cohen, P. J. Farmer, P. R. Ortiz de Montellano, *J. Am. Chem. Soc.* **2002**, *124*, 5684–5691.
[27] L. Ba, P. Li, H. Zhang, Y. Duan, Z. Lin, *Biotechnol. Bioeng.* **2013**; DOI: 10.1002/bit.24960.
[28] S. G. Bell, J. H. C. McMillan, J. A. Yorke, E. Kavanagh, E. O. D. Johnson, L.-L. Wong, *Chem. Commun.* **2012**, *48*, 11692–11694.
[29] T. L. Poulos, B. C. Finzel, A. J. Howard, *J. Mol. Biol.* **1987**, *195*, 687–700.
[30] I. F. Sevrioukova, C. Garcia, H. Li, B. Bhaskar, T. L. Poulos, *J. Mol. Biol.* **2003**, *333*, 377–392.
[31] I. F. Sevrioukova, H. Li, T. L. Poulos, *J. Mol. Biol.* **2004**, *336*, 889–902.
[32] W. Zhang, S. S. Pochapsky, T. C. Pochapsky, N. U. Jain, *J. Mol. Biol.* **2008**, *384*, 349–363.
[33] S. Tripathi, H. Li, T. L. Poulos, *Science* **2013**, *340*, 1227–1230.
[34] M. Holden, M. Mayhew, D. Bunk, A. Roitberg, V. Vilker, *J. Biol. Chem.* **1997**, *272*, 21720–21725.
[35] T. C. Pochapsky, T. A. Lyons, S. Kazanis, T. Arakaki, G. Ratnaswamy, *Biochimie* **1996**, *78*, 723–733.
[36] A. Karyakin, D. Motiejunas, R. C. Wade, C. Jung, *Biochim. Biophys. Acta Gen. Subj.* **2007**, *1770*, 420–431.
[37] J. D. Thompson, D. G. Higgins, T. J. Gibson, *Nucleic Acids Res.* **1994**, *22*, 4673–4680.
[38] Y. Yasutake, Y. Fujii, T. Nishioka, W.-K. Cheon, A. Arisawa, T. Tamura, *J. Biol. Chem.* **2010**, *285*, 31193–31201.
[39] D. H. Sherman, S. Li, L. V. Yermalitskaya, Y. Kim, J. A. Smith, M. R. Waterman, L. M. Podust, *J. Biol. Chem.* **2006**, *281*, 26289–26297.
[40] Y.-T. Lee, R. F. Wilson, I. Rupniewski, D. B. Goodin, *Biochemistry* **2010**, *49*, 3412–3419.
[41] C. Savino, L. C. Montemiglio, G. Sciara, A. E. Miele, S. G. Kendrew, P. Jemth, S. Gianni, B. Vallone, *J. Biol. Chem.* **2009**, *284*, 29170–29179.
[42] W.-C. Huang, A. C. G. Westlake, J.-D. Marechal, M. G. Joyce, P. C. E. Moody, G. C. K. Roberts, *J. Mol. Biol.* **2007**, *373*, 633–651.
[43] W. Yang, S. G. Bell, H. Wang, W. Zhou, N. Hoskins, A. Dale, M. Bartlam, L.-L. Wong, Z. Rao, *J. Biol. Chem.* **2010**, *285*, 27372–27384.
[44] N. Urushino, K. Yamamoto, N. Kagawa, S. Ikushiro, M. Kamakura, S. Yamada, S. Kato, K. Inouye, T. Sakaki, *Biochemistry* **2006**, *45*, 4405–4412.
[45] I. Wiedemann, R. Benz, H.-G. Sahl, *J. Bacteriol.* **2004**, *186*, 3259–3261.
[46] H. E. Hasper, B. de Kruijff, E. Breukink, *Biochemistry* **2004**, *43*, 11567–11575.
[47] T. Nagao, T. Mitamura, X. H. Wang, S. Negoro, T. Yomo, I. Urabe, H. Okada, *J. Bacteriol.* **1992**, *174*, 5013–5020.
[48] T. Nishioka, Y. Yasutake, Y. Nishiya, T. Tamura, *FEBS J.* **2012**, *279*, 3264–3275.
[49] K. I. Sallam, N. Tamura, T. Tamura, *Gene* **2007**, *386*, 173–182.
[50] Z. Shao, W. A. Dick, R. M. Behki, *Lett. Appl. Microbiol.* **1995**, *21*, 261–266.
[51] S. Nakashima, T. Tamura, *Appl. Environ. Microbiol.* **2004**, *70*, 5557–5568.
[52] A. Hemsley, N. Arnheim, M. D. Toney, G. Cortopassi, D. J. Galas, *Nucleic Acids Res.* **1989**, *17*, 6545–6551.
[53] T. Omura, R. Sato, *J. Biol. Chem.* **1964**, *239*, 2370–2378.
[54] V. Tiranti, C. Viscomi, T. Hildebrandt, I. Di Meo, R. Mineri, C. Tiveron, M. D. Levitt, A. Prelle, G. Fagiolari, M. Rimoldi, M. Zeviani, *Nat. Med.* **2009**, *15*, 200–205.
[55] A. Aliverti, B. Curti, M. A. Vanoni in *Methods in Molecular Biology, Vol. 131: Flavoprotein Protocols* (Eds.: S. K. Chapman, G. A. Reid), Humana, Totowa, **1999**, pp. 9–23.
[56] W. Kabsch, *Acta Crystallogr. Sect. D Biol. Crystallogr.* **2010**, *66*, 125–132.
[57] A. Vagin, A. Teplyakov, *J. Appl. Crystallogr.* **1997**, *30*, 1022–1025.
[58] G. N. Murshudov, A. A. Vagin, E. J. Dodson, *Acta Crystallogr. Sect. D Biol. Crystallogr.* **1997**, *53*, 240–255.
[59] P. Emsley, K. Cowtan, *Acta Crystallogr. Sect. D Biol. Crystallogr.* **2004**, *60*, 2126–2132.
[60] R. A. Laskowski, M. W. MacArthur, D. S. Moss, J. M. Thornton, *J. Appl. Crystallogr.* **1993**, *26*, 283–291.
[61] N. A. Baker, D. Sept, S. Joseph, M. J. Holst, J. A. McCammon, *Proc. Natl. Acad. Sci. USA* **2001**, *98*, 10037–10041.

Received: June 14, 2013
Published online on September 24, 2013

Acta Crystallographica Section F
Structural Biology and Crystallization Communications
ISSN 1744-3091

Crystallization and preliminary X-ray diffraction studies of D-*threo*-3-hydroxyaspartate dehydratase isolated from *Delftia* sp. HT23

Yu Matsumoto,[a] Yoshiaki Yasutake,[b]* Yuki Takeda,[a] Tomohiro Tamura,[b,c] Atsushi Yokota[a] and Masaru Wada[a]*

[a]Laboratory of Microbial Physiology, Research Faculty of Agriculture, Hokkaido University, Kita-9, Nishi-9, Kita-ku, Sapporo 060-8589, Japan, [b]Bioproduction Research Institute, National Institute of Advanced Industrial Science and Technology (AIST), 2-17-2-1 Tsukisamu-Higashi, Toyohira-ku, Sapporo 062-8517, Japan, and [c]Laboratory of Molecular Environmental Microbiology, Graduate School of Agriculture, Hokkaido University, Kita-9, Nishi-9, Kita-ku, Sapporo 060-8589, Japan

Correspondence e-mail: y-yasutake@aist.go.jp, wada@chem.agr.hokudai.ac.jp

Received 4 July 2013
Accepted 26 August 2013

D-*threo*-3-Hydroxyaspartate dehydratase (D-THA DH) isolated from the soil bacterium *Delftia* sp. HT23 is a novel enzyme consisting of 380 amino-acid residues which catalyzes the conversion of D-*threo*-3-hydroxyaspartate to oxaloacetate and ammonia. D-THA DH also catalyzes the dehydration of L-*threo*-3-hydroxyaspartate, L-*erythro*-3-hydroxyaspartate and D-serine. The amino-acid sequence of D-THA DH shows significant similarity to that of two eukaryotic D-serine dehydratases derived from *Saccharomyces cerevisiae* and chicken kidney. D-THA DH is classified into the fold-type III group of pyridoxal enzymes and is the first example of a fold-type III dehydratase derived from a prokaryote. Overexpression of recombinant D-THA DH was carried out using a *Rhodococcus erythropolis* expression system and the obtained protein was subsequently purified and crystallized. The crystals of D-THA DH belonged to space group $I4_122$, with unit-cell parameters $a = b = 157.3$, $c = 157.9$ Å. Single-wavelength anomalous diffraction data were collected to a resolution of 2.0 Å using synchrotron radiation at the wavelength of the Br K absorption edge.

1. Introduction

3-Hydroxyaspartate and its derivatives have biological activity as competitive blockers of excitatory glutamate/aspartate transporters of the mammalian nervous system (Balcar *et al.*, 1977; Shigeri *et al.*, 2001). Thus, pharmacological aspects of 3-hydroxyaspartate have attracted the attention of biochemists. 3-Hydroxyaspartate exists as four stereoisomers because it has two chiral centres, *i.e.* D-*threo*-3-hydroxyaspartate (2*R*,3*R*; D-THA), L-*threo*-3-hydroxyaspartate (2*S*,3*S*; L-THA), D-*erythro*-3-hydroxyaspartate (2*R*,3*S*; D-EHA) and L-*erythro*-3-hydroxyaspartate (2*S*,3*R*; L-EHA), which are difficult to synthesize individually (Kaneko & Katsura, 1963). For this reason, we considered that an enzyme that degrades 3-hydroxyaspartate might be useful for the enzymatic optical resolution of DL-racemic 3-hydroxyaspartate to produce optically pure 3-hydroxyaspartate isomers. However, there have been very few studies on enzymes that act on 3-hydroxyaspartate, although two bacterial enzymes, *erythro*-3-hydroxyaspartate aldolase (EC 4.1.3.14; Gibbs & Morris, 1964; Kornberg & Morris, 1965) and *erythro*-3-hydroxyaspartate dehydratase (EC 4.3.1.20; Gibbs & Morris, 1965), were identified many years ago.

In order to obtain amino-acid sequence information for 3-hydroxyaspartate dehydratase, we screened soil microorganisms that can utilize 3-hydroxyaspartate as a sole carbon source and recently found two novel enzymes in a newly isolated bacterium. One enzyme is an L-*threo*-3-hydroxyaspartate dehydratase (L-THA DH; EC 4.3.1.16; Wada *et al.*, 1999; Murakami *et al.*, 2009) isolated from *Pseudomonas* sp. T62, which only exhibits dehydratase activity towards L-THA. The other enzyme is a D-*threo*-3-hydroxyaspartate dehydratase (D-THA DH; EC 4.3.1.27; Maeda *et al.*, 2010) isolated from *Delftia* sp. HT23, which exhibits dehydratase activity towards D-THA, L-THA, L-EHA and D-serine.

Interestingly, although L-THA DH and D-THA DH catalyze the same reaction from *threo*-3-hydroxyaspartate to oxaloacetate and

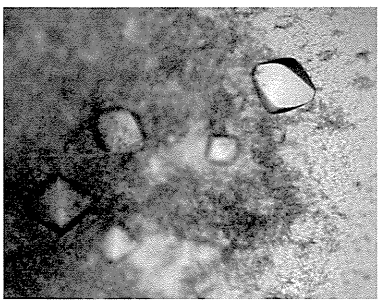

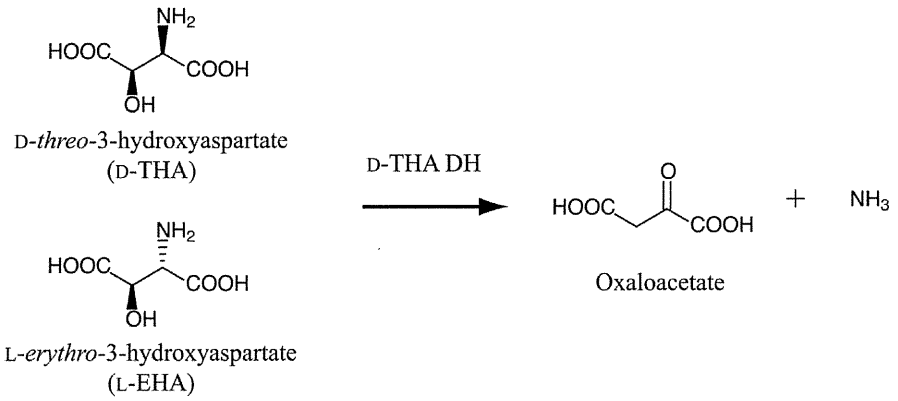

Figure 1
Scheme of the reactions catalyzed by D-*threo*-3-hydroxyaspartate dehydratase (D-THA DH).

ammonia, the primary structures of these two enzymes are completely different. Biochemical analyses suggested that both enzymes contain pyridoxal 5′-phosphate (PLP) as a cofactor. Based on their folding patterns, PLP-dependent enzymes are classified into five groups, designated fold-types I–V (Schneider *et al.*, 2000). A sequence-similarity search revealed that L-THA DH belongs to the fold-type II group, which contains most bacterial dehydratases. On the other hand, despite catalyzing the same dehydratase reactions, D-THA DH belongs to the fold-type III group, which contains most bacterial alanine racemases (Eliot & Kirsch, 2004). However, any alanine, serine or aspartate racemase activity of D-THA DH was below the detection limit. The amino-acid sequence of D-THA DH shows 26–36% similarity to two eukaryotic D-serine dehydratases derived from *Saccharomyces cerevisiae* (scDSD; Ito *et al.*, 2008) and chicken kidney (chDSD; Tanaka *et al.*, 2008), which are also classified into the fold-type III group. To the best of our knowledge, D-THA DH is the first example of a fold-type III dehydratase derived from a prokaryote.

Recently, the crystal structure of chDSD has been reported. This is the first report of the three-dimensional structure of a fold-type III enzyme that catalyzes a dehydratase reaction (Tanaka *et al.*, 2011). The primary structural similarity between D-THA DH and chDSD suggests that their active-site structures are similar. Nonetheless, D-THA DH shows unique stereospecificity towards 3-hydroxyaspartate isomers. The main substrate of chDSD is D-serine or D-threonine, which is the D-form of β-hydroxy amino acids. In contrast, the main substrate of D-THA DH is D-THA or L-EHA, *i.e.* not only the D-form but also the L-form of β-hydroxy amino acids act as a substrate for D-THA DH (Fig. 1). In other words, D-THA DH exhibits stringent stereoselectivity at C^{β} but relaxed selectivity at C^{α}, because D-THA and L-EHA have the same configuration around C^{β}. In the structure of chDSD, Zn^{2+} is located at the active site and is involved in the catalytic reaction (Tanaka *et al.*, 2011). D-THA DH pretreated with ethylenediaminetetraacetic acid (EDTA) also requires divalent cations for its activation, but the activation pattern differs between the two enzymes. Only Zn^{2+} and Mn^{2+} act as activators of chDSD, whereas Co^{2+}, Ni^{2+}, Ca^{2+} and Fe^{2+} ions are also activators of D-THA DH in addition to Zn^{2+} and Mn^{2+} ions. In particular, D-THA DH is highly activated by Mn^{2+}, Co^{2+} and Ni^{2+} ions, although the natural metal ion bound to D-THA DH has not yet been determined. To resolve the unique substrate specificity and to determine the properties contributing to the difference in their metal requirements, crystallographic studies of D-THA DH are required. Here, we report the improvement of the expression level, crystallization and preliminary X-ray diffraction studies of recombinant D-THA DH.

2. Materials and methods

2.1. Overexpression and purification of recombinant D-THA DH

The identification and cloning of the D-THA DH gene have been reported previously (Maeda *et al.*, 2010). Briefly, the gene encoding D-THA DH (GenBank accession code AB433986) was cloned from genomic DNA of *Delftia* sp. HT23 and inserted into the pQE30 expression vector using *Bam*HI and *Hin*dIII restriction enzymes. Recombinant D-THA DH was obtained by expression in *Escherichia coli* JM109 and used for enzymatic studies. For crystallization, recombinant D-THA DH was produced using *Rhodococcus erythropolis* as a host cell (Mitani *et al.*, 2005). The gene encoding D-THA DH was amplified using polymerase chain reaction (PCR) with a pQE30dthadh plasmid as template DNA, PrimeSTAR HS DNA polymerase (Takara Bio) and synthetic primers, *i.e.* forward (5′-AGTC**TCATGA**GTATGCAAGACACACTTCTGAC-3′) and reverse (5′-ATAT**CTCGAG**TCACCAGCCATGGAGCCGCT-3′). The bold bases indicate the *Bsp*HI and *Xho*I restriction sites, respectively. The PCR conditions were as follows: 30 cycles of amplification at 371 K for 10 s, at 333 K for 5 s and at 345 K for 1.5 min, followed by an elongation step at 345 K for 7 min. PCR fragments were digested with *Bsp*HI and *Xho*I and cloned into the *Nco*I and *Xho*I sites of the pTip-QC2 expression vector for *Rhodococcus* (Nakashima & Tamura, 2004*a*,*b*). *Bsp*HI, which is compatible with *Nco*I, was used for the digestion of the PCR fragments because the DNA sequence of the gene encoding D-THA DH contains an *Nco*I site. The resulting plasmid encoded full-length D-THA DH fused with a Met-Gly-His_6-Ala-Met-Ser sequence at the N-terminus. The plasmid was transformed into *R. erythropolis* L88 cells by electroporation.

The transformed cells were grown at 303 K in 50 ml Luria–Bertani (LB) medium containing 17 $\mu g\ ml^{-1}$ chloramphenicol. The preculture was then inoculated in 500 ml LB medium supplemented with 0.5 $\mu g\ ml^{-1}$ thiostrepton for 24 h at 303 K in order to induce D-THA DH expression. The cells were harvested (10 g wet weight) and resuspended in buffer *A* (10 m*M* Tris–HCl pH 8.0, 0.01 m*M* PLP, 0.1 m*M* dithiothreitol). The cells were disrupted three times using a French pressure cell (Ohtake Works) at 110 MPa after the addition of 2 $mg\ ml^{-1}$ lysozyme for 30 min. After centrifugation, the resulting supernatant was applied onto a His-Trap HP column (GE Healthcare) pre-equilibrated with buffer *A* which was supplemented with 20 m*M* imidazole and 500 m*M* NaCl. The enzyme was eluted with a linear gradient of 20–500 m*M* imidazole in buffer *A* supplemented with 500 m*M* NaCl. The fractions containing D-THA DH were collected, dialyzed against buffer *A* and subsequently concentrated to

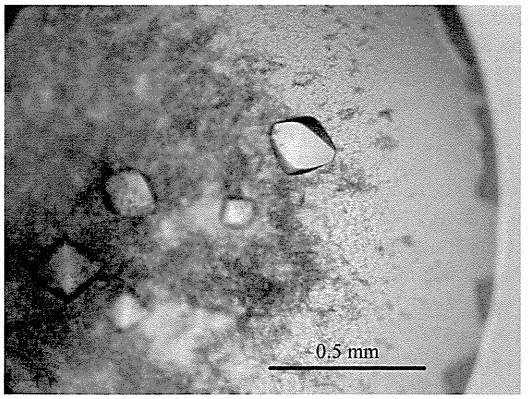

Figure 2
Typical crystals of D-*threo*-3-hydroxyaspartate dehydratase (D-THA DH). The crystal used for the current study was obtained with 0.1 *M* Tris pH 8.5, 0.2 *M* $MgCl_2$, 13% PEG 3350.

15 mg ml^{-1} using a centrifugal filtration device (10 000 Da molecular-weight cutoff, Millipore). The protein concentration was determined by the Bradford method using the Bio-Rad protein assay (Bio-Rad) with bovine serum albumin as the standard. The final protein solution consisted of 10 m*M* Tris–HCl pH 8.0, 0.01 m*M* PLP, 0.1 m*M* dithiothreitol and 15 mg ml^{-1} of the enzyme in a total volume of 0.7 ml.

2.2. Crystallization

Initial crystallization screening was performed in a 96-well crystallization plate by employing the sitting-drop vapour-diffusion technique at 293 K using commercially available sparse-matrix screen kits from Hampton Research and Emerald BioSystems. Each sitting drop was prepared by mixing 0.5 µl sample solution and 0.5 µl reservoir solution and was equilibrated against 100 µl reservoir solution. The most promising condition was subsequently optimized in a 24-well VDX plate (Hampton Research) by using the hanging-drop vapour-diffusion method at 293 K, with variation of the buffer pH and salt and precipitant concentrations. Each hanging drop was prepared by mixing 1.5 µl sample solution and an equal volume of the reservoir solution and was equilibrated against 500 µl reservoir solution.

2.3. X-ray diffraction studies

For X-ray diffraction under cryogenic conditions, crystals were soaked stepwise in cryoprotectant solution composed of crystallization reservoir and 20% glycerol. Subsequently, crystals were further transferred stepwise into cryoprotectant solution supplemented first with 0.5 *M* NaBr and then with 1 *M* NaBr, with an overall soaking time of approximately 30 s (Dauter *et al.*, 2000). Prior to X-ray diffraction analysis, the crystal was flash-cooled in a nitrogen-gas stream at 100 K. Single-wavelength anomalous diffraction (SAD) data were collected on beamline NW-12A at the Photon Factory (PF), Tsukuba, Japan using an ADSC Quantum 210 charge-coupled device detector. The wavelength was set at 0.91944 Å considering the results from a fluorescence scan around the Br *K* absorption edge. Each oscillation frame was taken with a rotation angle of 0.5° and an exposure time of 1.0 s. The total rotation range for the SAD data collection was 360°. The diffraction images were processed with *iMOSFLM*/*SCALA* (Battye *et al.*, 2011; Winn *et al.*, 2011). SAD phasing was performed with *SHELXC*/*D*/*E* (Sheldrick, 2008).

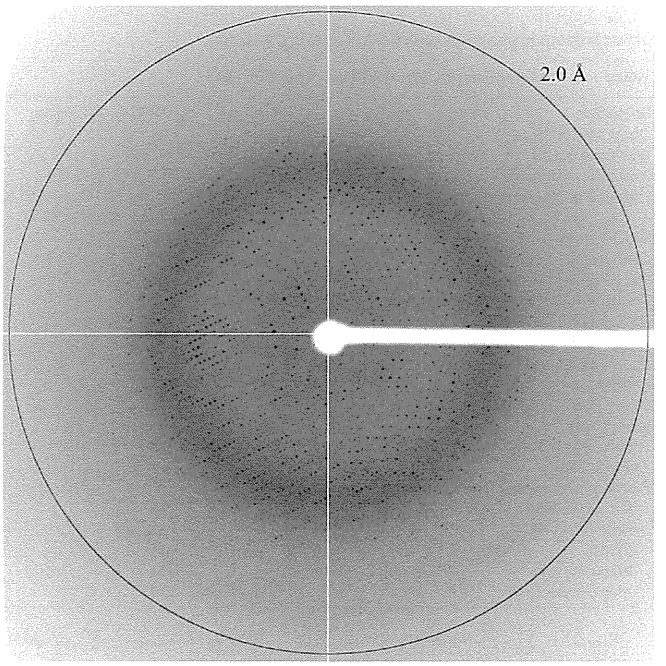

Figure 3
An X-ray diffraction pattern obtained on the NW-12A beamline at PF, Japan from a single crystal of D-*threo*-3-hydroxyaspartate dehydratase (D-THA DH).

2.4. Enzyme assay

3-Hydroxyaspartate dehydratase activity was assayed spectrophotometrically by measuring the change in absorbance of NADH at 340 nm using a DU800 spectrophotometer (Beckman Coulter). The assay was performed using a coupling system with NADH-dependent malate dehydrogenase (MDH) as described previously (Wada *et al.*, 1999). The standard assay mixture consisted of 100 m*M* Tris–HCl buffer pH 8.0, 0.01 m*M* PLP, 10 m*M* D-THA or L-EHA as a substrate, 0.32 m*M* NADH, 10 units of MDH and an appropriate amount of the enzyme in a total volume of 0.5 ml. The reactions were carried out at 303 K with addition of the substrate. Reaction mixtures without the substrate served as controls. One unit of the enzyme represented 1 µmol of NADH utilized per minute at 303 K on the basis of an absorption coefficient of 6.22 mM^{-1} cm^{-1} for NADH at 340 nm.

3. Results and discussion

The expression level of D-THA DH in *E. coli* was low, probably owing to the high GC content (71.9%) of the gene encoding D-THA DH. To address this problem, overexpression of recombinant D-THA DH was carried out using *R. erythropolis*, a Gram-positive bacterium with a high GC content (Actinobacteria), as a heterologous expression host. As shown by SDS–PAGE, we observed high expression of D-THA DH fused with additional Met-Gly-His_6-Ala-Met-Ser residues at the N-terminus in *R. erythropolis* (Supplementary Fig. S1[1]). As seen in lane 1, the molecular weight of recombinant D-THA DH was found to be 41.7 kDa, and that of the lysozyme added before the cell-disruption step was found to be 14.4 kDa. The specific activity of the cell-free extract of *R. erythropolis* expressing the D-THA DH gene was ~2.5 U per milligram of protein, which is about 20-fold higher

[1] Supplementary material has been deposited in the IUCr electronic archive (Reference: NO5025).

Table 1
Crystallographic parameters and SAD phasing statistics.

Values in parentheses are for the outermost resolution shell.

Beamline	NW-12A, PF, Japan
Temperature (K)	100
Wavelength (Å)	0.91944
Resolution range (Å)	50–2.0 (2.11–2.00)
Unit-cell parameters (Å, °)	$a = b = 157.3$, $c = 157.9$, $\alpha = \beta = \gamma = 90$
Space group	$I4_122$
Average mosaicity (°)	0.43
No. of reflections measured	1967835
No. of unique reflections measured	66655
R_{merge}†	0.149 (0.754)
R_{meas} (all $I+$ and $I-$)‡	0.157 (0.776)
$R_{p.i.m.}$ (all $I+$ and $I-$)§	0.029 (0.142)
Completeness (%)	100.0 (100.0)
Anomalous completeness (%)	100.0 (100.0)
Multiplicity	29.5 (29.8)
Anomalous multiplicity	15.4 (15.3)
Average $I/\sigma(I)$	24.4 (6.9)
Phasing information from *SHELXC/D/E*	
No. of Br sites used for phasing	42
Best CC_{all}/CC_{weak}	39.3/20.3
FOM	0.55
Map contrast	0.51
Map connectivity	0.90

† $R_{merge} = \sum_{hkl}\sum_i |I_i(hkl) - \langle I(hkl)\rangle| / \sum_{hkl}\sum_i I_i(hkl)$. ‡ $R_{meas} = \sum_{hkl}\{N(hkl)/[N(hkl)-1]\}^{1/2}\sum_i |I_i(hkl) - \langle I(hkl)\rangle| / \sum_{hkl}\sum_i I_i(hkl)$. § $R_{p.i.m.} = \sum_{hkl}\{1/[N(hkl)-1]\}^{1/2}\sum_i |I_i(hkl) - \langle I(hkl)\rangle| / \sum_{hkl}\sum_i I_i(hkl)$, where $I_i(hkl)$ is the ith intensity measurement of reflection hkl, $\langle I(hkl)\rangle$ is the mean intensity of reflection hkl and $N(hkl)$ is the number of observations of reflection hkl.

than that of the cell-free extract of *E. coli* expressing the D-THA DH gene. D-THA DH was purified by Ni-affinity chromatography, resulting in a single band on SDS–PAGE (Supplementary Fig. S1). The calculated molecular weight of the protein with the additional residues is determined to be 41 629 Da, which is consistent with the molecular weight determined by SDS–PAGE. The theoretical isoelectric point of the recombinant protein was calculated to be 6.32. This procedure yielded approximately 10 mg purified D-THA DH per 500 ml of culture.

Diffraction-quality crystals were obtained with a reservoir solution consisting of 0.1 *M* Tris pH 8.5, 0.2 *M* $MgCl_2$, 10–14% PEG 3350. Yellow-coloured crystals appeared in the heavy precipitate and grew to approximate dimensions of 0.2 × 0.2 × 0.2 mm within 1 week (Fig. 2). The Br-SAD data set was collected to a resolution of 2.0 Å using synchrotron radiation at a wavelength of 0.91944 Å (Fig. 3). Preliminary data processing showed that the unit-cell parameters were close to $a = b = c = 158$ Å, $\alpha = \beta = \gamma = 90°$. Thus, the data were integrated and scaled assuming that the crystal belonged to a cubic space group. However, abnormally high R_{merge} values were calculated for any cubic system, suggesting that the crystal did not have three-fold symmetry around the cube diagonal. Therefore, we reduced the symmetry and found that the crystal belonged to an *I*-centred tetragonal space group with a reliable R_{merge} value. The reflection condition for (00*l*) indicated that the true space group of the crystal was $I4_122$ with unit-cell parameters $a = b = 157.3$, $c = 157.9$ Å. Assuming the presence of two D-THA DH monomers in the asymmetric unit, the calculated value of the crystal volume per protein weight (V_M value; Matthews, 1968) was 2.8 $Å^3\ Da^{-1}$. This value corresponds to a solvent content of 56.4%. SAD phasing was performed using *SHELXC/D/E* (Sheldrick, 2008). A total of 42 Br sites were found using the data with a resolution range of 20–2.8 Å. SAD phasing and density modification using *SHELXE* resulted in an interpretable electron-density map. X-ray diffraction data collection and phasing statistics are summarized in Table 1. Model building and refinement are currently under way.

The authors would like to thank the beamline scientists at the Photon Factory, Tsukuba, Japan for their kind assistance in the X-ray diffraction experiment. This work was financially supported in part by a grant-in-aid from the Institute for Fermentation, Osaka (IFO).

References

Balcar, V. J., Johnston, G. A. & Twitchin, B. (1977). *J. Neurochem.* **28**, 1145–1146.
Battye, T. G. G., Kontogiannis, L., Johnson, O., Powell, H. R. & Leslie, A. G. W. (2011). *Acta Cryst.* D**67**, 271–281.
Dauter, Z., Dauter, M. & Rajashankar, K. R. (2000). *Acta Cryst.* D**56**, 232–237.
Eliot, A. C. & Kirsch, J. F. (2004). *Annu. Rev. Biochem.* **73**, 383–415.
Gibbs, R. G. & Morris, J. G. (1964). *Biochim. Biophys. Acta*, **85**, 501–503.
Gibbs, R. G. & Morris, J. G. (1965). *Biochem. J.* **97**, 547–554.
Ito, T., Hemmi, H., Kataoka, K., Mukai, Y. & Yoshimura, T. (2008). *Biochem. J.* **409**, 399–406.
Kaneko, T. & Katsura, H. (1963). *Bull. Chem. Soc. Jpn*, **36**, 899–903.
Kornberg, H. L. & Morris, J. G. (1965). *Biochem. J.* **95**, 577–586.
Maeda, T., Takeda, Y., Murakami, T., Yokota, A. & Wada, M. (2010). *J. Biochem.* **148**, 705–712.
Matthews, B. W. (1968). *J. Mol. Biol.* **33**, 491–497.
Mitani, Y., Meng, X., Kamagata, Y. & Tamura, T. (2005). *J. Bacteriol.* **187**, 2582–2591.
Murakami, T., Maeda, T., Yokota, A. & Wada, M. (2009). *J. Biochem.* **145**, 661–668.
Nakashima, T. & Tamura, T. (2004*a*). *Appl. Environ. Microbiol.* **70**, 5557–5568.
Nakashima, T. & Tamura, T. (2004*b*). *Biotechnol. Bioeng.* **86**, 136–148.
Schneider, G., Käck, H. & Lindqvist, Y. (2000). *Structure*, **8**, R1–R6.
Sheldrick, G. M. (2008). *Acta Cryst.* A**64**, 112–122.
Shigeri, Y., Shimamoto, K., Yasuda-Kamatani, Y., Seal, R. P., Yumoto, N., Nakajima, T. & Amara, S. G. (2001). *J. Neurochem.* **79**, 297–302.
Tanaka, H., Senda, M., Venugopalan, N., Yamamoto, A., Senda, T., Ishida, T. & Horiike, K. (2011). *J. Biol. Chem.* **286**, 27548–27558.
Tanaka, H., Yamamoto, A., Ishida, T. & Horiike, K. (2008). *J. Biochem.* **143**, 49–57.
Wada, M., Matsumoto, T., Nakamori, S., Sakamoto, M., Kataoka, M., Liu, J.-Q., Itoh, N., Yamada, H. & Shimizu, S. (1999). *FEMS Microbiol. Lett.* **179**, 147–151.
Winn, M. D. *et al.* (2011). *Acta Cryst.* D**67**, 235–242.

FEBS Letters 588 (2014) 105–110

ELSEVIER

FEBS Letters

journal homepage: www.FEBSLetters.org

1964–2014

Structure of the quinoline N-hydroxylating cytochrome P450 RauA, an essential enzyme that confers antibiotic activity on aurachin alkaloids

Yoshiaki Yasutake [a,*], Wataru Kitagawa [a,b], Miyako Hata [a], Taiki Nishioka [b], Taro Ozaki [c,1], Makoto Nishiyama [c], Tomohisa Kuzuyama [c], Tomohiro Tamura [a,b]

[a] Bioproduction Research Institute, National Institute of Advanced Industrial Science and Technology (AIST), 2-17-2-1 Tsukisamu-Higashi, Toyohira-ku, Sapporo 062-8517, Japan
[b] Graduate School of Agriculture, Hokkaido University, Kita-9, Nishi-9, Kita-ku, Sapporo 060-8589, Japan
[c] Biotechnology Research Center, The University of Tokyo, 1-1-1 Yayoi, Bunkyo-ku, Tokyo 113-8657, Japan

ARTICLE INFO

Article history:
Received 7 October 2013
Revised 6 November 2013
Accepted 6 November 2013
Available online 20 November 2013

Edited by Miguel De la Rosa

Keywords:
Cytochrome P450
CYP
Aurachin
Antibiotic
Menaquinone
Rhodococcus erythropolis

ABSTRACT

The cytochrome P450 RauA from *Rhodococcus erythropolis* JCM 6824 catalyzes the hydroxylation of a nitrogen atom in the quinolone ring of aurachin, thereby conferring strong antibiotic activity on the aurachin alkaloid. Here, we report the crystal structure of RauA in complex with its substrate, a biosynthetic intermediate of aurachin RE. Clear electron density showed that the quinolone ring is oriented parallel to the porphyrin plane of the heme cofactor, while the farnesyl chain curls into a U-shape topology and is buried inside the solvent-inaccessible hydrophobic interior of RauA. The nearest atom from the heme iron is the quinolone nitrogen (4.3 Å), which is consistent with RauA catalyzing the N-hydroxylation of the quinolone ring to produce mature aurachin RE.

1. Introduction

Antibiotics play an important role in the treatment of severe bacterial infections. Investigations into new antibiotic regimens are required because of the emergence of multi-drug resistance, as well as new pathogenic bacteria. Aurachin alkaloids are rare compounds found in nature and are composed of a quinolone ring and farnesyl chain. Two phylogenetically unrelated bacterial species, *Rhodococcus* and *Stigmatella*, are known to synthesize several molecular variations of aurachin alkaloids [1–7]. A previous study indicated that aurachins could be potent inhibitors of mitochondrial respiration because of their structural similarity with menaquinone (vitamin K_2), the sole respiratory quinone for most eubacteria [8]. The enzymes that catalyze the synthesis of menaquinone are potential targets for the development of novel antibacterial drugs [9].

Aurachin RE is an aurachin alkaloid isolated from *Rhodococcus erythropolis* JCM 6824 (Fig. 1), and it exhibits relatively strong antibiotic activity against a wide range of gram-positive bacteria [6]. Recent studies revealed that aurachin RE exhibits inhibitory activity against 1,4-dihydroxy-2-naphthoate prenyltransferase (MenA) of *Mycobacterium tuberculosis*, which is an essential enzyme in the menaquinone biosynthesis pathway [10–12]. Therefore, the antibiotic property of aurachin RE might be caused by the inhibition of menaquinone biosynthesis as well as the respiratory chain reaction itself [12]. We recently identified the operon for aurachin RE biosynthesis (*rauA–rauH*) of *R. erythropolis* JCM 6824, and gene disruption experiments revealed that *rauA*, which encodes a cytochrome P450 monooxygenase, is crucial for its antibiotic activity [7]. In addition, we found that recombinant P450 RauA catalyzes nitrogen hydroxylation of the quinolone ring and produces the mature antibiotic aurachin RE. Therefore, RauA is considered to be the final enzyme that completes the biosynthesis of aurachin RE [7]. Interestingly, the P450 gene functionally corresponding to RauA has not been found in the genome sequence of *Stigmatella aurantiaca* Sg a15 [4], and thus, RauA is likely a unique entity specifically evolved for the recognition of the aurachin skeleton in *R. erythropolis*.

P450s are heme-containing enzymes widely found in eukaryotes, bacteria, and archaea and play a role in diverse biological functions, such as biosynthesis of steroids, lipids, antibiotics, detoxification of xenobiotics, and drug metabolism [13]. A typical

Abbreviations: CYP, cytochrome P450 monooxygenase; RMSD, root–mean–square deviation; HPLC, high-performance liquid chromatography

* Corresponding author. Fax: +81 11 857 8980.
E-mail address: y-yasutake@aist.go.jp (Y. Yasutake).
[1] Graduate School of Agricultural and Life Sciences, The University of Tokyo, 1-1-1 Yayoi, Bunkyo-ku, Tokyo 113-8657, Japan.

0014-5793/$36.00
http://dx.doi.org/10.1016/j.febslet.2013.11.016

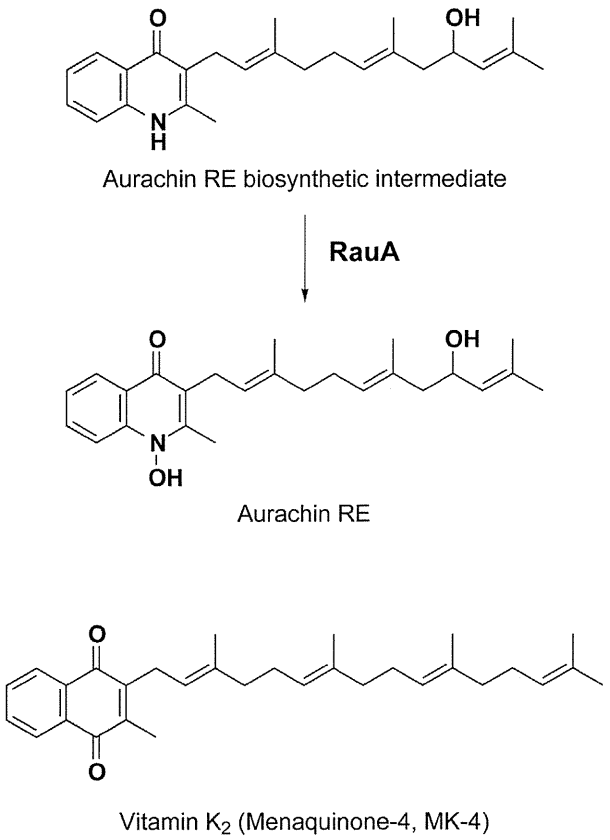

Fig. 1. Enzymatic reaction catalyzed by RauA. Aurachin RE biosynthetic intermediate is the substrate for RauA. The structure of vitamin K_2 (Menaquinone-4, MK-4) is also shown. The figure was created using ChemDraw (CambridgeSoft).

reaction catalyzed by P450s is monooxygenation, i.e., insertion of an activated oxygen atom generated from molecular oxygen (O_2) into the substrate compound using two electrons sequentially delivered from the redox partner protein and an additional two protons [14]. P450s form a conserved 3D structure known as the "P450-fold"; however, the substrate-binding pocket in the vicinity of the heme cofactor has evolved to accommodate a wide variety of compounds. In bacteria, most P450s are distributed in actinomycetes and are considered to be involved in the biosynthesis of certain secondary metabolites, including antibiotics, and metabolism of exogenous compounds. Currently, a number of P450 genes have been identified because of the recent advances in genome analysis. However, the biological function, substrate specificity, and 3D structures of most P450s remain unknown.

Here, we report the enzymatic and structural characterization of a new bacterial P450, RauA. Since aurachins are rare compounds found in nature, it is of interest to elucidate how RauA recognizes the aurachin skeleton. RauA is also unique in that it catalyzes the hydroxylation of the cyclic nitrogen atom, although some P450s are known to catalyze N-hydroxylation of amines or amidines [15,16]. Our structure clearly showed that the aurachin RE intermediate is buried inside the active-site pocket with the nitrogen atom of its quinolone moiety oriented toward the heme iron.

2. Materials and methods

2.1. Overexpression and purification of RauA

Gene cloning and analysis of recombinant protein expression were performed according to a previously described method [7]. Briefly, the *rauA* gene was cloned into the *Nde*I and *Xho*I sites of the pET26 expression vector, and the recombinant RauA containing a C-terminal His_6-tag was expressed in *Escherichia coli* BL21-CodonPlus(DE3)-RIL cells. The expression of RauA was induced with 0.1 mM isopropyl β-D-thiogalactopyranoside in LB medium supplemented with $FeSO_4$ (100 μM) and 5-aminolevulinic acid (80 μg/ml) [17]. The RauA was purified by Ni-affinity chromatography followed by anion-exchange chromatography [7]. For crystallization, the purity was increased by gel-filtration chromatography with a Sephacryl S-100 column (GE-Healthcare) using a solution containing 20 mM Tris pH 7.5, 150 mM NaCl, and 10% glycerol. A carbon monoxide binding assay [18] was performed to verify the RauA concentration.

2.2. Enzyme activity measurement and kinetic analysis

Aurachin RE biosynthetic intermediate (substrate) was obtained from the culture media of *rauA* gene disruption mutant strain of *R. erythropolis* as previously described [7]. The enzyme assay was performed with reconstitution experiments. The reaction mixture contained 1.0–2.5 μM RauA, 1.0–20.0 μM substrate, 100 μg/ml spinach ferredoxin (Fdx) (Sigma–Aldrich), 0.1 U/ml spinach ferredoxin reductase (FdxR) (Sigma–Aldrich), 3 U/ml D-glucose dehydrogenase (TOYOBO), 2 mM NADPH, and 60 mM D-glucose in a total volume of 200 μl of reaction buffer (50 mM Tris–HCl, pH 7.5). After pre-incubation at 30 °C for 2 min, the reaction was initiated by the addition of NADPH, followed by incubation at 30 °C for the appropriate period (2–5 min). The reaction was terminated by extracting once with 800 μl of ethyl acetate. The resulting organic extract was dried and re-dissolved in 100 μl of methanol. The methanol solution was analyzed by HPLC (high-performance liquid chromatography) using the same procedure as previously described [7]. The molar quantity of aurachin RE and its intermediate was estimated on the basis of the previously reported molar absorption coefficient for aurachin D at one of its major absorption peaks (334 nm) [1]. The K_m and k_{cat} values were estimated from Michaelis–Menten kinetics using the KaleidaGraph (Synergy Software), after triplicate experiments with varying substrate concentrations.

2.3. Substrate binding assay

The substrate-induced spectral shift was monitored using a JASCO V-630 spectrophotometer with a 1-cm path length quartz cell. The aurachin RE intermediate (substrate) was dissolved in dimethyl sulfoxide (DMSO) at concentrations ranging from 0 to 10 μM, and 10 μl of the substrate solution was added to 990 μl of a reaction mixture containing 2.5 μM RauA and 20 mM Tris–HCl, pH 7.5. Spectral titrations with 0–10 μM substrate were performed at 25 °C. The equation $\Delta A = \Delta A_{max}([S]/([S] + K_d))$ was fitted to the experimental data using the nonlinear least squares fitting program (SOLVER; http://www.solver.com/), where [S] is the free substrate concentration. The [S] was obtained as $[S] = [S]_{total} - [ES] = [S]_{total} - ([E]\Delta A/\Delta A_{max})$, where $[S]_{total}$ is the total concentration of substrate, [ES] is the concentration of enzyme–substrate complex, and [E] is the total concentration of enzyme [19].

2.4. Crystallization

All crystallization experiments were performed at 293 K using the vapor-diffusion technique. Prior to crystallization, the protein solution was pre-incubated overnight at 277 K with a 10-fold molar excess of substrate. The protein solution was mixed with an equal volume of precipitant solution and equilibrated against the reservoir containing the same precipitant solution. RauA was crystallized using a precipitant solution containing 0.1 M MES pH